1 **Designing bifunctional catalysts for urea electrolysis: Progresses and**

2 **perspectives**

3

4

5

Abstract

Urea electrolysis becomes an attractive method for sustainable energy-saving hydrogen production and simultaneous pollutant degradation. To improve urea electrolysis efficiency and simplify the electrolysis systems, developing efficient bifunctional electrocatalysts arouses great interest. Recently, great achievements have been made in the design of high-performance bifunctional catalysts for urea electrolysis. In this review, current progress in bifunctional catalysts for urea electrolysis is comprehensively analyzed. Urea electrolysis fundamentals and catalyst design principles are first discussed. Then, the applications of advanced bifunctional catalysts in urea electrolysis are fully demonstrated, such as single atom catalysts (SACs), metal nanoparticles, alloys, metal (hydr)oxides, chalcogenides, pnictides, metal-organic frameworks (MOFs), composites, etc. The structure-performance correlation of catalysts is emphasized, as well as design strategies. Current catalysts are also benchmarked in terms of their catalytic activities, for providing insights into the sensible design of high-performance bifunctional electrocatalysts. Several Key perspectives are outlined to guide further studies on practical urea electrolysis-driven sustainable hydrogen production and urea-rich wastewater management.

Please check a similarity report.

1. Introduction

Urea $(CO(NH_2)_2)$ is a widely used organic chemical in synthetic chemistry, agriculture, automobile systems, medicine, etc.[1,2] The widespread usage of urea generates a lot of urea-bearing wastewater. Also, human/animal excrement contains a high level of urea. The disorderly discharge of such urea-rich effluents leads to serious environmental pollution issues (e.g., eutrophication, NO_x gaseous pollutants) and a waste of nitrogen resources.[3,4] Therefore, making a green use of urea-rich effluents would alleviate the related environmental problems and accelerate the global nitrogen cycle.

Recently, electrooxidation of urea under mild conditions has gained souring interest, which can convert urea into CO_2, N_2, and water in an efficient manner. Importantly, urea oxidation reaction (UOR) is thermodynamically more favorable than oxygen evolution reaction (OER), the anodic half-reaction of water electrolysis.[5] It is thus sensible to couple hydrogen evolution reaction (HER) with UOR to accomplish energy-saving hydrogen fuel production. However, the slow kinetics of both HER and UOR hinders the hydrogen production efficiency via urea electrolysis.[6] For improving the economic attractiveness of urea electrolysis systems, it is favored to perform both HER and UOR in a same electrolyte. Therefore, many attempts have been employed to develop high-performance catalysts/electrodes towards urea electrolysis in alkaline media. To further simplify the manufacture of electrolyzers and electrodes for HER and UOR, designing bifunctional catalysts is highly recommended.

To date, diverse bifunctional electrocatalysts based on low-priced metals (e.g., Ni, Co, Fe) and precious metals (e.g., Rh, Pt, Ru) have been developed for urea electrolysis.[7,8] From SACs, metal nanoparticles, and alloys to metal (hydr)oxides, chalcogenides, and pnictides, catalysts with

3

46   diverse nanostructures and compositions have exhibited good performance towards urea

47   electrolysis, as listed in **Table S1** (Supporting information). Current efforts focus on tailoring the

48   internal and external properties (size, nanostructure, surface chemistry, electronic structure) of

49   catalysts to meet the multiple requirements of urea electrolysis, and thus a series of catalyst design

50   strategies have been developed, like heteroatom doping,[9] composite construction,[10] vacancy

51   engineering,[11] nanostructure control[12]. These achievements significantly promote the development

52   of bifunctional catalysts for urea electrolysis and take a closer step towards practical urea-rich

53   wastewater electrolysis for energy-saving hydrogen production. Nevertheless, an inclusive review

54   summing up advances in bifunctional electrocatalysts for urea electrolysis remains unavailable,

55   although many reviews have summarized the electrocatalysts for UOR (mainly Ni-based

56   materials).[2, 13-23]

57   Herein, this review aims at providing a thorough analysis of current developments in the

58   bifunctional electrocatalysts for the electrolysis of urea solutions. Fundamentals of urea

59   electrolysis and electrocatalyst design principles are first discussed. The applications of

60   bifunctional catalysts in urea electrolysis are fully demonstrated, including SACs, metal

61   nanoparticles, alloys, metal (hydr)oxides, chalcogenides, pnictides, MOFs, composites, etc. For

62   guiding the future development of high-performance bifunctional catalysts, we have benchmarked

63   current catalysts in terms of their catalytic activities. At last, several perspectives are put forward

64   to guiding further studies in the field of urea electrolysis.

65   2. Fundamentals of urea electrolysis

66   Urea electrolysis, consisting of anodic UOR and cathodic HER, can be used to realize energy-

67   efficient hydrogen production and simultaneous urea pollutant degradation. Generally, urea

68 electrolysis is performed in 1 M KOH alkaline electrolyte in the presence of urea (in most cases,

69 0.1-0.5 M). As shown in **Fig. 1a**, urea electrolysis takes a significant smaller theoretical potential

70 of 0.37 V for hydrogen generation than conventional water splitting (1.23 V), indicating a feasible

71 route towards sustainable hydrogen production from urea-based wastewater. For bifunctional

72 catalysts for urea electrolysis, good performance towards both HER and UOR is required.

73 **2.1. HER mechanism**

74 Mechanism investigations for the cathodic HER process in alkaline electrolytes gain great interest.

75 The HER will undergo the Volmer-Heyrovsky pathway or the Volmer-Tafel pathway (**Fig. 1b**),

76 which is generally determined by the value of calculated Tafel slope derived from linear sweep

77 voltammetry (LSV) curves. The Tafel slopes of the Tafel, Heyrovsky, and Volmer reactions are

78 around 30, 40, and 120 mV dec^{-1} respectively. Accordingly, when Tafel slopes of catalysts fall with

79 the range of 40-120 mV dec^{-1}, a Volmer-Heyrovsky mechanism is suggested. Of note, different

80 from HER in acidic media which store rich H$^+$ ions, alkaline HER starts from the

81 adsorption/dissociation of H$_2$O on catalyst surface. In this context, water adsorption energy, water

82 dissociation energy, and H* adsorption-free energy are critical activity indicators in computational

83 studies.

84 Recently, it has been suggested that transition metal-based catalysts would undergo structure

85 reconstruction during HER with the formation of metal hydroxide phases on catalyst surface. For

86 instance, chalcogenide anions of metal chalcogenides can be readily replaced by OH$^-$ in highly

87 alkaline electrolytes, thereby generating metal hydroxide on the surface of metal chalcogenides.[24]

88 The metal hydroxide species on the chalcogenide/hydroxide composite has been found to help

89 dissociate water molecules and elevate catalytic performance.[25]

5

2.2. UOR mechanism

The electrooxidation of UOR is a complicated process, in terms of the diversity in reaction conditions, catalysts, and oxidation products.[2, 13, 14] To date, most bifunctional electrocatalysts for alkaline urea electrolysis are based on transition metals (especially Ni), with main products of CO_2, N_2, and H_2O. In this part, the UOR process over Ni-based catalysts are discussed, and a representative mechanism is illustrated in **Fig. 1c**.[13] Firstly, *in situ* generation of NiOOH phase on catalyst surface under the alkaline and oxidative conditions is suggested, which acts as real UOR active sites. The generated NiOOH then can react with the urea molecule and provide electroactive sites for further intermediate adsorption/desorption/rearrangement, new chemical bond formation, and finally leads to the conversion of urea into CO_2, N_2 and H_2O. As depicted in **Fig. 1c**, two N-N coupling pathways are put forward for possible N_2 formation mechanism, and it remains challenging to directly determine a clear mechanism for UOR over a typical catalyst.

The self-oxidation degree of transition metal catalysts during UOR governs the understanding of real active sites. For catalysts that undergo complete *in situ* electrooxidation, the parent catalyst phase will entirely transform into a metal (oxy)hydroxide phase which determines UOR performance.[26] Differently, partial electrooxidation of original catalysts would lead to an active core@shell nanostructure for UOR. Thus, it is necessary to thoroughly investigate structure self-evolution of catalysts during UOR process, and gains insights of real active sites for UOR. Aside from most Ni^{3+}-based NiOOH active phase, a Ni^{4+} active site-involved UOR pathway has been suggested by Zhang et al.,[27] which exhibits better UOR performance than NiOOH-involved process. Over a β-$Ni(OH)_2$ catalyst, Chen and co-authors suggested that a spontaneous urea molecule dehydrogenation mechanism, including six proton-coupled electron transfer processes, hydration, as well as reactant rearrangement.[28] Recently, Wang et al. developed a Co and Ge, co-

113   doped Ni oxyhydroxide catalyst to convert urea into nitrite, which attained a Faradaic efficiency

114   of 84.9% at 1.4 V vs reversible hydrogen electrode (RHE).[29] These interesting results indicate that

115   it is too early to get a general conclusion on the UOR mechanism, and more studies are suggested

116   to uncover the catalyst-dependent mechanism with detailed experimental and computational tools.

117
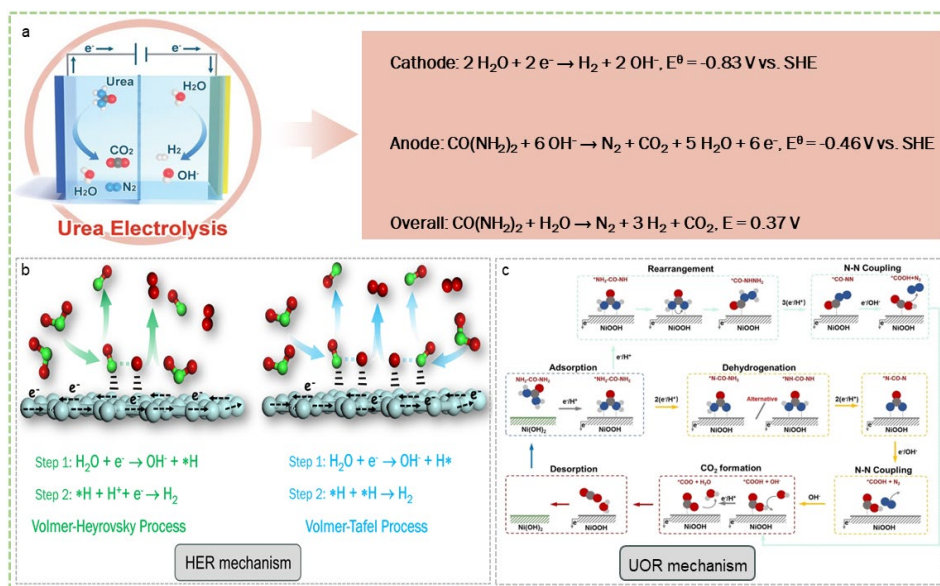
118   **Fig. 1** (a) Scheme of urea electrolysis process and the reaction equations.[15] (b) HER mechanism. (a) A possible UOR

119   mechanism.[13]

3. Design principles of bifunctional electrocatalysts for urea electrolysis

121   Electrocatalysts' activity and stability are critical for their practical application in urea electrolysis

122   (**Fig. 2**). In general, the catalytic activity of electrocatalysts is governed by the intrinsic activity of

123   per electroactive site and the amount of exposed catalytic electroactive sites. In addition, the HER

124   and UOR of urea electrolysis are interfacial reactions in electrolytes, and thus the fast charge

125 transfer/mass transport process at the gas-liquid-solid triphasic interface is essential to improve the

126 performance. Besides activity, working stability of catalysts is another factor that determines their

127 feasibility of real application, which is largely affected by the nanostructure and fabrication process

128 of electrodes.

3.1. High intrinsic activity

130 Fundamentally, the intrinsic activity of electrocatalysts is determined by their electronic properties.

131 Thus, adjusting the electronic structure of catalysts becomes a powerful tool for enhancing

132 catalytic performance. Through regulating catalysts' chemical composition, phase structure,

133 crystallinity, and introducing heteroatom dopants, defects/vacancies, it is sensible to reconstruct

134 the electronic structure of catalysts. Also, developing heterostructures which contain two or more

135 active components can lead to the interfacial interaction between different components, which can

136 also help to regulate electronic properties of host materials. For example, in the CoS_2/MoS_2

137 Schottky heterojunction, spontaneous charge transfer between MoS_2 and CoS_2 induces the

138 generation of separated nucleophilic/electrophilic regions.[30] The modulated surface charge

139 distribution synergistically promotes the adsorption and break of urea molecules during UOR.

140 These practical strategies have been well illustrated for effectively boosting the intrinsic activity

141 of catalysts by reshaping the electronic properties.

142 Another route to boost the intrinsic catalytic activity of materials is introducing additional

143 electroactive phases, which can be achieved by heterostructure construction. The combination of

144 multiple active sites would help to boost diverse reaction steps (e.g., water adsorption/dissociation,

145 urea adsorption, hydrogen evolution, urea splitting, CO_2 and N_2 generation and desorption) during

146 urea electrolysis. Typically, following the modular design principle, it is suggested to integrate a

147 HER active material with a UOR active material into one electrocatalyst, with the aim of realizing

148 overall urea electrolysis.

149 **3.2. High density of active sites**

150 To ensure an efficient catalytic reaction process, it is necessary to provide high density of

151 electroactive sites on catalyst surface. For particle-shape electrocatalysts, decreasing the

152 agglomeration of particles is important for exposing more active sites; also, downsizing can

153 populate the electroactive sites. Both size/agglomeration reduction can be achieved by

154 nanostructure control, which relates to the detailed investigation of synthetic parameters.

155 Heteroatom doping, amorphization, and crystal facet engineering are also suggested to increase

156 the active sites. Typically, amorphous structures with flexible atomic arrangement and rich edge

157 sites are expected to possess higher density of active sites than the crystalline counterparts.[31]

158 Constructing nanostructures with large specific surface area (SSA) and porosity is a commonly

159 applied strategy to populate active sites. For example, nanowires, nanospheres, nanotubes,

160 nanosheets, hollow structures, multi-channel structures, porous structures, core@shell structures,

161 and hierarchical structures are excellent for their high interconnected active area.

162 **3.3. Efficient mass/charge transfer**

163 As a gas generation process in electrolytes, urea electrolysis needs high mass transport and charge

164 transfer efficiencies. Designing open structures (e.g., nanoarrays, multi-channel structures,

165 hierarchical structures) with interconnected active surface is a good option to accelerate the

166 electrolyte penetration and the diffusion of reactants/intermediates, which also helps the interfacial

167 charge transfer during electrochemical reactions. The development of self-supported open

168 structures is especially important for large-current density urea electrolysis, because of the

169 generation of huge number of gaseous products. Additionally, by applying highly conductive

170 carbon materials (such as carbon nanotubes (CNTs), graphene, N-doped carbon) into catalysts, it

171 is expected to construct an efficient charge transfer pathway among different components and

172 thereby accelerate the charge transfer process.

173 **3.4. Long working stability**

174 To meet the potential industrial application, robust electrodes with long-term stability are required.

175 For binder-involved electrodes, the working stability can be regulated by using stable chemical

176 components and by nanostructure control of catalysts. For example, using a carbon cover on Ni

177 particles is suggested to enhance the electrode stability by limiting the inactivation and

178 electrochemical etching of active Ni species.[32] Also, the binder/catalyst ratio and other electrode

179 fabrication parameters influence the operating performance of electrodes.

180 Alternatively, one can directly design binder-free electrodes in which active components are self-

181 supported by conductive substrates, like nickel foam, nickel/iron foam, and carbon cloth. The

182 direct construction of active catalysts on substrates shows tight connection between the two

183 components, and thus enhances the mechanical stability. The self-supported electrodes also can

184 avoid the general active component shedding issue in binder-based electrodes. In addition, such

185 integrated electrodes show a simple preparation process and can save the electrode fabrication cost.
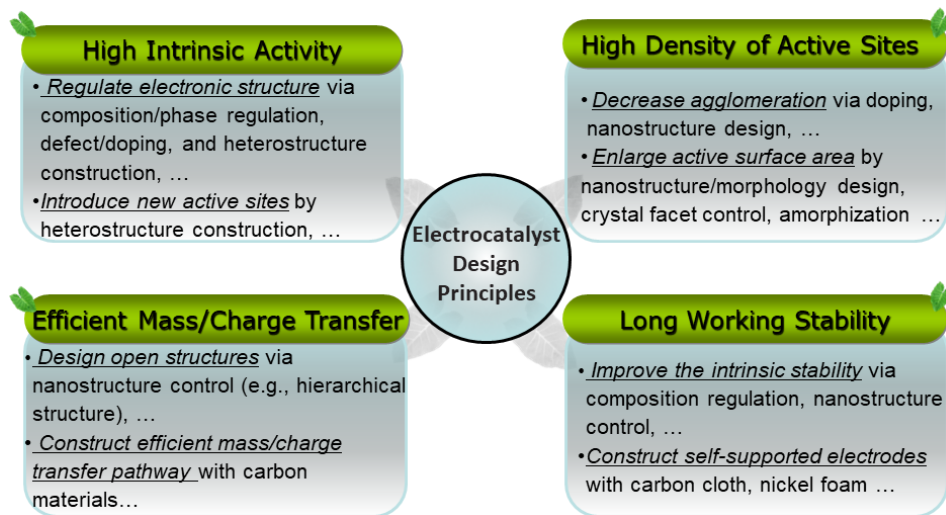
Fig.2 Electrocatalyst design principles for urea electrolysis.

4. Applications of bifunctional electrocatalysts for urea electrolysis

Recently, hundreds of bifunctional electrocatalysts have been developed for urea electrolysis, including SACs, metal nanoparticles, alloys, metal (hydr)oxides, chalcogenides, pnictides, MOFs, composites, etc. Most of these catalysts are fabricated based on Ni and Co, because of their high activity and low price. In this section, currently reported bifunctional catalysts are comprehensively analyzed, and the rational design of bifunctional catalysts is emphasized and outlined in **Table 1**.

Table 1 Representative bifunctional catalysts for urea electrolysis.

Category	Electrocatalyst	Key design strategy	Electrolyte	E_{10}^{a} (V)
	Ni@NCDs[32]	Composite construction	1 M KOH + 0.5 M urea	1.47

Metals and alloys	Ni-Mo alloy nanotube array[7]	Nanostructure control	1 M KOH + 0.1 M urea	1.43
	Ni-NiO-MoNi[33]	Composite construction	1 M KOH + 0.5 M urea	1.37
	Rh/NiV-LDH[34]	Single-atom catalyst	1 M KOH + 0.33 M urea	1.47 (E_{100})
Metal oxides	CoFe$_2$O$_4$ nanoneedle[11]	Nanostructure control, vacancy engineering	1 M KOH + 0.33 M urea	1.47
	Ru/P co-doped NiMoO$_4$[35]	Dual doping	1 M KOH + 0.5 M urea	1.73 (E_{500})
	Ni$_3$S$_2$–NiMoO$_4$[36]	Composite construction, phase engineering	1 M KOH + 0.5 M urea	1.61 (E_{500})
	NiMoO$_4$/Ni$_3$S$_4$/MoS$_2$[37]	Composite construction, nanostructure control	1 M KOH + 0.5 M urea	1.55 (E_{50})
Metal hydroxides	Co-doped Ni(OH)$_2$[38]	Doping	1 M KOH + 0.5 M urea	1.42
	CoN/Ni(OH)$_2$[39]	Composite construction	1 M KOH + 0.5 M urea	1.43
	P-doped NiCoZn LDH[b 40]	Doping, nanostructure control	1 M KOH + 0.5 M urea	1.479 (E_{100})
Metal chalcogenides	NiCo$_2$S$_4$ nanosheets[41]	Nanostructure control	1 M KOH + 0.33 M urea	1.49
	Fe-doped Ni$_3$S$_2$[42]	Doping	1 M KOH + 0.33 M urea	1.49
	Se/NiSe$_2$[43]	Composite construction (Schottky heterojunction)	1 M KOH + 0.33 M urea	1.59
	Amorphous Ni-S-Se[44]	Phase engineering	1 M KOH + 0.5 M urea	1.47
	Ni$_3$S$_2$@CoMoS$_4$/NiFeOOH[45]	Composite construction	1 M KOH + 0.5 M urea	1.66 (E_{100})
Metal pnictides	Ni$_3$N nanosheets[46]	Nanostructure control	1 M KOH + 0.5 M urea	1.503 (E_{100})
	Hollow NiCoP nanoprisms[47]	Component optimization, nanostructure control	1 M KOH + 0.5 M urea	1.36
	Mo, Fe co-doped Co$_2$P[48]	Dual doping	1 M KOH + 0.5 M urea	1.415
	Ni$_3$N/Ni$_{0.2}$Mo$_{0.8}$N nanorod arrays[49]	Composite construction, nanostructure control	1 M KOH + 0.5 M urea	1.348

	CoS$_x$/Co-MOF[50]	Composite construction, nanostructure control	1 M KOH + 0.5 M urea	1.48
Others	Fe-doped Ni MOF nanosheet arrays[51]	Nanostructure control, doping	1 M KOH + 0.33 M urea	1.431
	Ni-Co-B nanoparticles[52]	Component optimization	1 M KOH + 0.33 M urea	1.34
	NiF$_3$/Ni$_2$P[53]	Composite construction	1 M KOH + 0.33 M urea	1.54

Note: [a]E_{10}: applied potential at a current density of 10 mA cm^{-2} for urea electrolysis; [b]LDH: layered double hydroxide

4.1. Metal nanoparticles, and alloys

Metallic catalysts, with high electronic conductivity, are efficient for diverse electrochemical reactions. Ni has high intrinsic activity for UOR and HER,[54] while the aggregation of Ni nanoparticles during the conventional pyrolysis process significantly limits the electroactive area and leads to low catalytic performance. To address this issue, some studies focus on engineering Ni-based precursors with isolated Ni ions. Oxygen-based functional groups on carbon materials can provide rich binding sites for Ni^{2+}, and the pyrolysis of Ni^{2+}-carbon complexes can lead to Ni/carbon composite material with highly dispersed Ni nanoparticles.[32] In alkaline electrolytes, carbon also provides a protective cover for Ni active sites by limiting the leaching and inactivation of Ni. Another mainstream route to prepare isolated Ni nanoparticles is designing MOF-based precursors, in which Ni^{2+} can be separated by organic ligands. In 2018, Wang et al. developed a Zn/Ni-BTC (BTC: 1,3,5-trimesic acid) MOF as a precursor of the Ni/C catalyst.[55] After a calcination process, the obtained Ni/C catalyst shows a high Brunauer–Emmett–Teller (BET) specific surface area (SSA, 438 m^2 g^{-1}) and a high pore volume (0.605 cm^3 g^{-1}). Using for urea electrolysis, the bifunctional Ni/C can attain 10 mA cm^{-2} at 1.6 V.

212 Alloying is a powerful strategy to raise metals' intrinsic activity via tuning their electronic

213 properties. Several bimetallic alloys have exhibited favourable performance towards urea

214 electrolysis, such as AuRh,[56] $Cu_{0.5}Ni_{0.5}$,[57] and Ni-Mo alloy[7]. Although the noble metal-based AuRh

215 catalyst has an excellent activity for urea electrolysis (E_{100} = 1.47 V),[56] the high price of Au and

216 Rh would limit its practical applications. Alternatively, Ni-based low-cost alloys attract growing

217 interest. With a facile electrodeposition process, Zhang and coauthors developed a metastable

218 $Cu_{0.5}Ni_{0.5}$ alloy which has a nanoparticle structure (**Fig. 3a-b**).[57] Benefitting from the strong

219 electronic interaction between Cu and Ni and the metastable feature, $Cu_{0.5}Ni_{0.5}$ alloy/NF shows

220 high performance towards both HER and UOR. Especially, the $Cu_{0.5}Ni_{0.5}$ alloy is more favourable

221 for the *in situ* structure reconstruction during UOR process and can generate electroactive NiOOH

222 phase at lower potentials than bare Ni (**Fig. 3c**). The bifunctional $Cu_{0.5}Ni_{0.5}$ alloy/NF can save 305

223 mV at 100 mA cm^{-2} for urea electrolysis than for water electrolysis (**Fig. 3d**), indicating an energy-

224 saving hydrogen production process.

225 Designing composite materials include alloy/carbon and alloy/metal compound composites can

226 enhance the performance of alloys. The intention for constructing alloy/carbon composites is to

227 improve the dispersion of active alloy particles and improve the conductivity of catalysts. N-doped

228 carbon[58] and ordered mesoporous carbon[59] are thus developed for supporting Ni-based alloys.

229 Coupling alloys with another electroactive material can help to improve the intrinsic activity. It is

230 suggested that low-valence metal species in alloys are highly effective for HER,[60] while high-

231 valent metal species can facilitate *in situ* evolution of metal oxyhydroxide phases during UOR.[61]

232 In this context, metal oxides and sulfides have been extensively studied to promote catalytic

233 activities of alloys. Interestingly, Wang et al. created a $CoMn/CoMn_2O_4$ composite directly from

234 $CoMn_2O_4$ with a facile electrochemical treatment (**Fig. 3e**), which is composed of nanoflake arrays

14

235   (**Fig. 3f**).[62] Aside from the generation of multiple active sites, spontaneous charge transfer at the

236   CoMn/CoMn$_2$O$_4$ Schottky heterostructure interface promotes reactant absorption and chemical

237   bonds breaking, thereby initiating the splitting of urea and water (**Fig. 3g**). The bifunctional

238   CoMn/CoMn$_2$O$_4$ catalyst can efficiently catalyze urea electrolysis (E_{10} = 1.51 V), and realizes

239   energy-saving hydrogen production compared with water electrolysis (E_{10} = 1.64 V) (**Fig. 3h-i**).

240   Composites like MoNi$_4$/MoO$_x$@NF,[63] Ni-NiO-MoNi,[33] MoNiFeS$_x$@FeNi$_3$,[64] and

241   NiMo@ZnO/NF[65] also exhibit good performance towards urea electrolysis. In this studies, the

242   importance of multi-valence of metal species[63] and nanostructure[33, 65] in determining the catalytic

243   performance has been outlined.
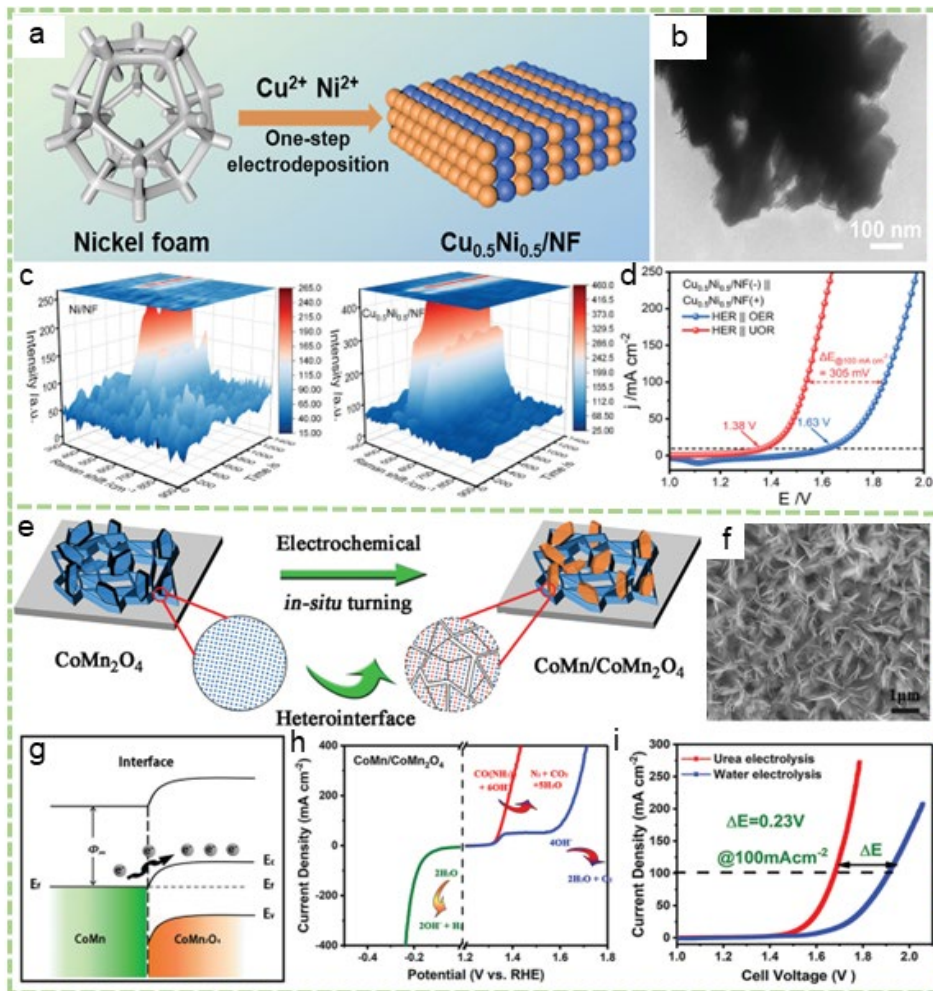
Fig. 3. (a) Scheme of the preparation of $Cu_{0.5}Ni_{0.5}/NF$ preparation. (b) TEM image of $Cu_{0.5}Ni_{0.5}/NF$. (c) *In situ* Raman spectra of $Cu_{0.5}Ni_{0.5}/NF$ and Ni/NF during UOR. (d) LSV curves of $Cu_{0.5}Ni_{0.5}/NF||Cu_{0.5}Ni_{0.5}/NF$ couple for water electrolysis and urea electrolysis.[57] (e) Schematic of the fabrication of $CoMn/CoMn_2O_4$. (f) SEM image of $CoMn/CoMn_2O_4$. (g) Energy band profile of $CoMn_2O_4$ and metallic CoMn after Schottky contact. (h) LSV curves of $CoMn/CoMn_2O_4$ for UOR, OER, and HER. (i) Polarization curves of $CoMn/CoMn_2O_4||CoMn/CoMn_2O_4$ for water electrolysis and urea electrolysis.[62]

16

4.2. Metal oxides

Transition metal oxides are widely used in electrocatalysis due to their high activity, eco-friendliness, facile preparation, and low cost. For urea electrolysis, a series of Ni and Co-based oxides have been developed. Catalysts-based on $Ni(Co)MoO_x$ are the most frequently reported because of dual active sites of Ni/Co and Mo for urea electrolysis.[66] Representatively, in the $Co_2Mo_3O_8$ catalyst, the high-valence Mo^{6+} species and the *in situ* generated Co_3O_4 phase contribute to the high UOR.[67] In terms of HER, the Co atom is responsible for breaking H-OH bond and the Mo site acts as hydrogen evolution center. The combination of Co and Mo in the oxide thus leads to a synergistic effect for urea electrolysis.

The catalytic properties of metal oxides generally can be regulated by oxygen vacancy construction and heteroatom doping. Oxygen vacancy can be easily introduced by a facile reduction treatment[11] or chemical etching[68]. The oxygen-deficient oxides can provide better HER and UOR performance than the pristine one. Zhang et al. suggested that oxygen vacancy in $CoFe_2O_4$ can boost the electrical conductivity of catalyst,[11] while how the oxygen vacancy tune the elemental reaction steps of urea electrolysis has not been studied. Heteroatom doping also holds great promise for improving oxides' catalytic activities. Metal dopants like Fe and V have been investigated to regulate the properties of $NiCo_2O_4$[69] and Co_3O_4[70], respectively. Beyond single doping, dual doping seems to be more effective. Ni, N-codoped $NiMoO_4$[71] and Ru/P dual-doped $NiMoO_4$[35] have exhibited upgraded performance for urea electrolysis than their single-doping counterparts. Guo found that the Ru, P dual-doping finely modulated the *d*-band center of $NiMoO_4$, thereby optimizing adsorption/desorption behavior of reaction intermediates.[35]

17

272 Constructing oxide-based composite catalysts is another efficient method. Integrating metal oxides

273 with metal particles,[72] alloys,[73] oxides,[74] sulfides,[75] phosphides,[76] and carbon materials[77] have been

274 explored. The introduction of carbon materials can improve the conductivity of catalysts and the

275 interaction between oxides and carbon ensures long-term stability.[78] In terms of metallic materials,

276 their combination with oxides can not only raise the conductivity but also provide new active sites.

277 In the $Ni/NiMoO_x$ electrocatalyst, the interface between Ni and $NiMoO_x$ benefits the conductivity

278 and modulates the surface polarization of the catalyst, thereby enhancing the UOR activity.[72] The

279 beneficial effect of the coupling interface between metallic sites and meta oxides is also found in

280 the CoMoO@Co composite,[79] $Ni@C–V_2O_3/NF$,[80] and $FeNi_3-MoO_2$[73]. Considering the success of

281 metal oxides/carbon and metal/metal oxides, developing tricomponent metal/metal oxides/carbon

282 composites becomes a sensible choice. As reported, Xu and coworkers designed a Ni/NiO hybrid

283 on N-doped carbon spheres (CA-Ni/NiO@NCS) by the two-step hydrothermal process-

284 carbonization method (**Fig. 4a**).[81] The TEM image shows that the well dispersion of nanosized

285 Ni/NiO particles on the carbon support (**Fig. 4b**), and an amorphous NiO-crystalline Ni interface

286 can be observed from the HRTEM images (**Fig. 4c-d**). Noting, the rich amorphous/crystalline

287 interface is able to adjust the electronic structure of the composite and thus optimize

288 absorption/desorption behavior of reactants and reaction intermediates. Also, abundant unsaturated

289 edge sites on the amorphous phase will provide highly active sites and promote the mass/charge

290 transport during electrochemical reactions (**Fig. 4e**). As such, the composite exhibits good

291 activities for urea electrolysis, with an E_{10} of 1.475 V (**Fig. 4f**).

292 Metal oxide/metal X (X = O, S, P) composites hold promise for urea electrolysis. The incorporation

293 of metal X components can improve metal oxides' performance in multiple ways, in terms of

294 intrinsic activity, active sites, and stability. For example, Xu et al. suggested that the CrO_x in

18

Ni/NiO@CrO$_x$ could accelerate the *in situ* evolution of NiOOH phase and provide a protective effect to enhance the stability for UOR.[82] In a tricomponent NiMoO$_4$/Ni$_3$S$_4$/MoS$_2$, the synergistic effect between Ni, Mo, and S with diverse valences favors both UOR and HER, and a low potential of 1.55 V is needed for attaining 50 mA cm^{-2}.[37] It is interesting to find that coupling metal oxides with components having other functions can form novel electrocatalytic systems. Jiang and coauthors combined sulfur-doped NiMoO$_4$ with plasmonic MoO$_2$ (S-NiMo/NF) for solar thermoelectric self-powered urea electrolysis.[83] The S-NiMo/NF composite has good plasmonic absorption and photothermal conversion abilities, which offers the opportunity of designing photothermal-assisted urea electrolysis. When integrated with a solar thermoelectric generator (STEG), the system can realize self-powered thermoelectric urea electrolysis with a high H$_2$ generation rate of over 160 μmol h^{-1}. In another Ni-modified WO$_3$/g-C$_3$N$_4$ composite (WO/CN–Ni@CF), both WO$_3$ and g-C$_3$N$_4$ have well-confirmed photocatalytic performance. Thus, the bifunctional WO/CN–Ni@CF driven photoelectrochemical urea electrolysis can save energy (0.3 V at E_{100}) for hydrogen production than the conventional electrochemical process.[84] By developing external field (e.g., heat, light)-responsive functional composites, such attempts can reduce the energy cost of urea electrolysis by utilizing solar energy.
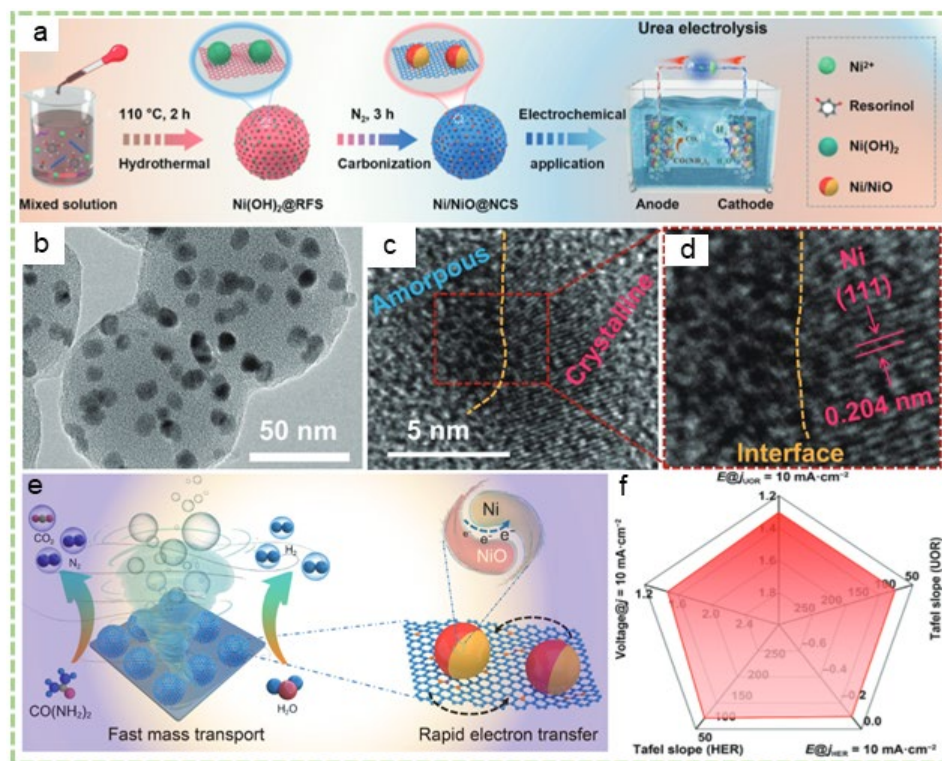
Fig. 4. (a) Schematic of the preparation of CA−Ni/NiO@NCS (CA: crystalline/amorphous). (b) TEM and (c, d) HTREM images of CA−Ni/NiO@NCS. (e) Scheme of the performance interpretation for CA−Ni/NiO@NCS. (f) Comprehensive catalytic activities of CA−Ni/NiO@NCS.[81]

4.3. Metal hydroxides

With a lamellar two-dimensional (2D) structure, metal layered double hydroxides (LDHs) are extensively applied in electrocatalysis. Aside from the 2D structure, the merit of facile preparation, flexible composition, and low toxicity make LDHs good catalysts for diverse applications. However, similar to metal oxides, the low conductivity of LDHs hinders their applications. In addition, the limited catalytic edge sites of LDHs are another unfavorable factor as electrocatalysts.

20

Current efforts have focused on addressing these issues by phase regulation, nanostructure control, vacancy introduction, elemental doping, and composite construction. For instance, the amorphous NiFeCo LDH/NF can catalyze urea electrolysis at 1.49 V (10 mA cm^{-2}), and the amorphous nature enhances the performance by affording high electrochemically active surface area (ESCA) and accelerating charge transport.[85] Tian et al. emphasized the importance of hierarchical quaternary superstructure of NiCo-LDH in urea electrolysis.[86] The three-dimensional (3D) hierarchical structure can expose rich active sites and accelerate mass/charge transfer.

To improve the intrinsic activities of LDHs, building oxygen vacancies and heteroatom doping gain much attention. The presence of holes on NiFe-LDHs leads to rich oxygen vacancies, which further help to expose more electroactive sites and regulate catalysts' electronic structure.[87] Via a plasma treatment, Yao et al. successfully constructed oxygen vacancies on a N-doped Ni-Fe oxyhydroxide.[88] The oxygen vacancy-doping dual-engineered catalyst can drive 10 mA cm^{-2} at 1.37 V. Density functional theory (DFT) calculations indicate oxygen vacancy and nitrogen dopant boost catalytic performance by increasing the conductivity of Ni-Fe oxyhydroxide. In a Ru-doped NiFe-LDH (NiFeRh-LDH) synthesized via a hydrothermal method (**Fig. 5a**), oxygen vacancies are also found.[89] The NiFeRh-LDH shows an interconnected nanosheets nanostructure (**Fig. 5b**). Further analysis suggests that urea molecules favor to adsorb on the oxygen vacancy-rich NiFeRh-LDH, and an optimized urea adsorption energy can be obtained on the Rh-doped LDH catalyst. With these advantages, NiFeRh-LDH can attain high activity and stability (**Fig. 5c-e**) for the electrolysis of pure urea solution and real urine wastewater (E_{10} = 1.35 V). Besides regulating the electronic properties of LDHs, metal dopants (e.g., Co) also can accelerate the *in situ* conversion of α-Ni(OH)$_2$ to NiOOH during UOR, thereby enhancing the catalytic performance.[38]

Another method to upgrade the catalytic performance of LDHs is constructing heterostructures. Aiming at improving the conductivity and alleviate the activity of LDHs, carbon, metal nanoparticles and metal oxides/sulfides/phosphides/nitrides have been introduced.[39, 90-93] Carbon materials like multiwalled carbon nanotubes (MWCNTs)[91] and fullerene quantum dots[94] can help to compensate the conductivity of LDHs, and importantly, fullerene quantum dots are suggested to precisely tune electronic properties of CoNi-LDH and thereby favor rection intermediate adsorption during urea electrolysis. The coupling of metal-bearing components with LDHs also can provide active sites and optimize catalysts' electronic properties. Gao et al. found that the electron transfer between $Ni(OH)_2$ and Ni favors urea adsorption,[90] while WO_3 in the $Ni(OH)_2/NiO-C/WO_3$ composite can transform Ni centers into highly active species for both HER and UOR[95]. In the amorphous P-doped FeOOH/crystalline NiFe phosphide ($P-NiFeO_xH_y$) composite array structure prepared by a corrosion-phosphorization method (**Fig. 5f-g**), the crystalline NiFe phosphide is tightly combined with the amorphous FeOOH (**Fig. 5h**).[96] In the multiphase composite, NiFeP provides abundant active sites and high electronic conductivity, amorphous P-doped FeOOH enhances the adsorption of oxygen-containing reactants/intermediates. In addition, the amorphous/crystalline structure together with the superaerophobic and superhydrophilic surface forms a synergistic effect, leading to rich active sites and enhanced mass/charge transfer. Combining with the photovoltaic equipment, the bifunctional $P-NiFeO_xH_y$ driven urea electrolysis system can respond speedily and realize stable hydrogen production without additional voltage input (**Fig. 5i-j**).
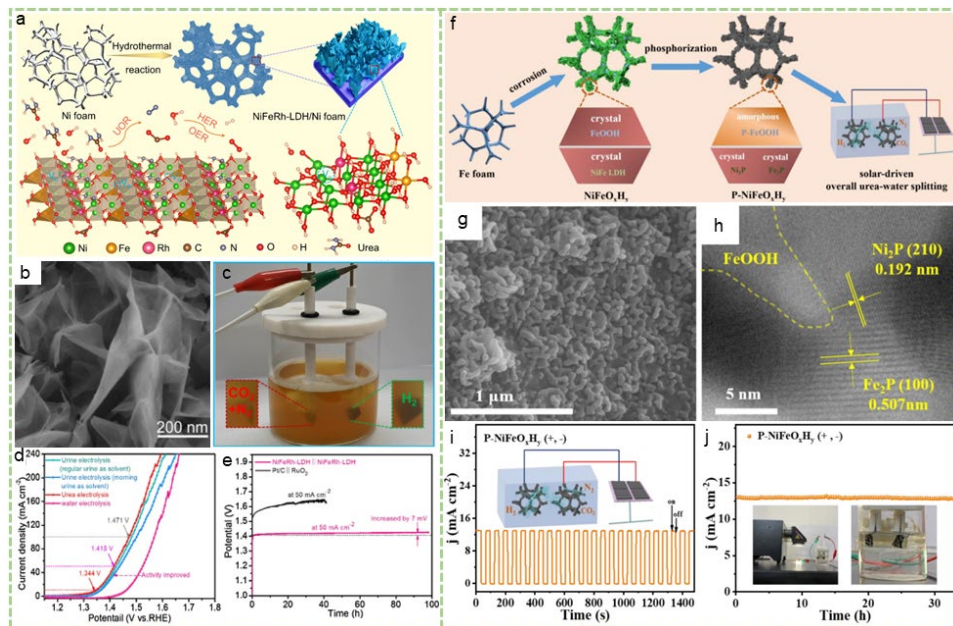
Fig. 5. (a) Scheme of the synthesis of Ru-doped NiFe-LDH. (b) SEM image of Ru-doped NiFe-LDH. (c) Picture of the urea electrolytic reactor. (d) LSV curves of water electrolysis, urine electrolysis, and urea electrolysis. (e) Urea electrolysis stability of bifunctional Ru-doped NiFe-LDH and commercial RuO_2||Pt/C couple.[89] (f) Illustration of the preparation of P-NiFeO$_x$H$_y$. (g) SEM and (h) TEM images of P-NiFeO$_x$H$_y$. (i) J-t profile under chopped illumination, inset shows an illustration of solar-driven urea electrolysis system. (d) Stability test of a solar cell-driven urea electrolysis.[96]

4.4. Metal chalcogenides

Metal chalcogenides (i.e., sulfides, selenides, and tellurides) are a group of promising electrocatalysts for urea electrolysis owing to their metallic feature and unique electronic structure.[97, 98] To develop high-performance metal chalcogenide catalysts, researchers have made efforts for enlarging active surface area by nanostructure control and enhancing intrinsic activity by phase regulation, heteroatom doping, and composite construction.

23

376 Limited active sites are a main issue that hinders the catalytic performance of electrocatalysts,

377 which can be well alleviated by nanostructure control. Compared with nanoparticles, metal sulfide

378 arrays developed by hydrothermal process-involved methods gain growing interest. To date, CoS_2

379 nanoneedle array,[99] $CoNi_2S_4$ nanosheets,[100] porous $NiCo_2S_4$ nanosheet array,[41] Ni-Co-S nanosheet

380 array,[101] Fe-Ni sulfide nanoarray,[102] Ni_3S_2 nanowires,[103] caterpillar-like $NiCo_2S_4$ array,[104] and SnS

381 nanosheet array[105] have been developed for urea electrolysis. By vertically loading $CoNi_2S_4$

382 nanosheets on wood cell walls, Jiang and coauthors suggested that the 3D hierarchical porous

383 wood framework and ultrathin $CoNi_2S_4$ nanosheets synergistically provides abundant catalytic

384 active sites, expedites mass/charge transfer, and accelerates the diffusion of gaseous products

385 during the electrochemical reactions.[100] Another route to engineer catalysts with high surface area

386 is using MOF-based precursors. Starting from a hierarchical PBA@MOF-Ni (Ni-Co Prussian blue

387 analogue on MOF-Ni) hybrid, Xu et al. developed a Co-Ni/Se with a solvothermal method.[106] The

388 obtained Co-Ni/Se shows a hollow nanocube structure and maintains the flower shape of the

389 precursor. Working as a bifunctional catalyst, Co-Ni/Se just takes 1.49 V at 10 mA cm^{-2}. A cobalt-

390 based MOF (ZIF67)/$Co(OH)_2$ nanosheet composite also has been used as a precursor for designing

391 yolk-shell $CoSe_2$ nanostructure.[107] These finely tuned nanostructures generally possess large SSA

392 and well-exposed active sites on the interconnected structure, which could accelerate mass/charge

393 transfer and reinforce the diffusion of electrolytes and gas bubbles during urea electrolysis, which

394 is extremely important for the operating situation under high current densities.

395 Amorphous chalcogenides have rich dangling bonds and unsaturated atoms which are highly

396 active sites for electrochemical reactions. Generally, the flexible electronic structure of amorphous

397 materials makes them more active than their crystalline counterpart. Thus, several amorphous

398 chalcogenides have been designed for urea electrolysis, like electrodeposited amorphous Ni-Mo-

399 S film,[108] porous and amorphous $CoS_x(OH)_y$,[109] and amorphous Ni-S-Se[44]. Chen and co-authors

400 recently developed amorphous Ni sulfide (Ni-S), selenide (Ni-Se), and sulfoselenide (Ni-S-Se) via

401 a two-step process (**Fig. 6a**).[44] The Ni-S-Se catalyst is composed of nanoplate array (**Fig. 6b**), and

402 the X-ray diffraction (XRD) patterns suggest an amorphous state (**Fig. 6c**). Ni-S-Se has a higher

403 *p*-band center for S than Ni-S (**Fig. 6d**); thus, S sites in Ni-S-Se have a stronger adsorption strength

404 of H* intermediate than that in Ni-S. Such electronic property leads to a better HER performance

405 of Ni-S-Se. In addition, the hybridization of electrons from Se, S, and Ni benefits electron

406 interaction/transfer between different active sites (**Fig. 6e**), contributing to high activity towards

407 UOR and HER. The bifunctional Ni-S-Se can drive urea electrolysis to realize an energy efficient

408 hydrogen production (**Fig. 6f-g**). Although this study has employed DFT calculations to explain

409 amorphous Ni-S-Se catalyst's high activity, one should keep in mind that building a precise crystal

410 model for amorphous materials remains a challenge and it is thus important to carefully check the

411 structure rationality of amorphous catalysts.

412 Heteroatom doping can alter the electronic structure of metal chalcogenides, and thus alleviate the

413 intrinsic activity for urea electrolysis.[110] Liu et al. found that the doping of Fe into Ni_3S_2 could

414 modify the coordination structure of Ni atoms and further optimize adsorption energies of reaction

415 intermediates on Ni sites.[42] In another study, the Fe dopant in a hydrothermally synthesized

416 hierarchical Ni_3S_2 electrode (**Fig. 6h-i**) is suggested to limit S dissolution and accelerate catalyst

417 reconstruction during electrochemical process.[111] Also, Fe dopant help to optimize the adsorption

418 of intermediates and push the *d*-band center to the Fermi level, facilitating catalytic reactions. As

419 a result, the Fe-Ni_3S_2 only takes 1.57 V at 100 mA cm^{-2}, and shows high stability over 500 h (**Fig.**

420 **6j-k**). Aside from tuning electronic properties, doping can also reshape the nanostructure of nickel

421 sulfides. Compared with Ni_3S_2 nanosheets, the Mo-doped Ni_3S_2 shows a morphology of branch-

422 like nanorods due to the anisotropic growth of MoO_4^{2-} during the hydrothermal process.[112] Thus,

423 the Mo-doped Ni_3S_2 has more active sites for urea electrolysis. Similarly, Mn dopant exhibits a

424 positive effect on the morphology of Ni–Se prepared by electrodeposition, and the Mn-

425 incorporated catalyst also benefits from the enhanced electrons transfer from Mn to Ni, thereby

426 leading to a better adsorption strength of reactants and intermediates.[113]
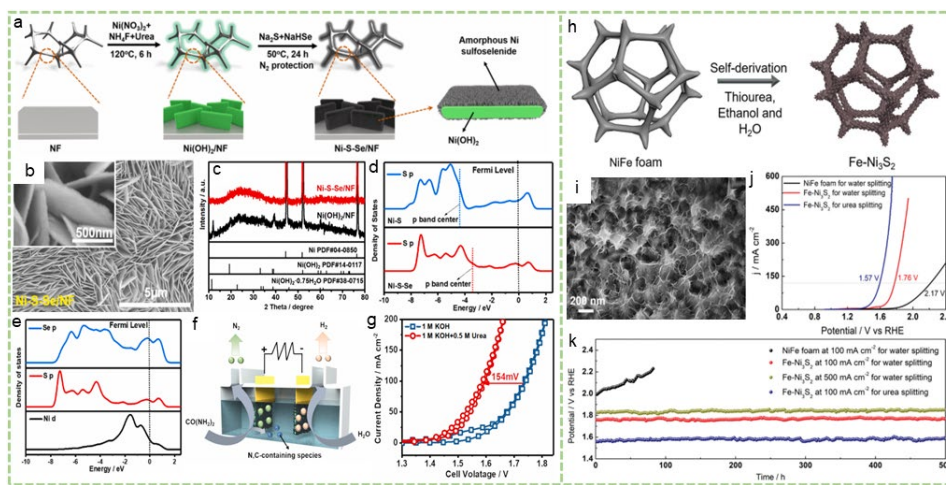
Fig .6 (a) Schematic of the synthesis of Ni-S-Se. (b) SEM image and (c) XRD patterns of Ni-S-Se. (d) Density of state (DOS) of S's p orbital for Ni-S-Se and Ni-S. (e) DOS of Se p, S p, and Ni d orbitals for Ni-S-Se. (f) Scheme of a urea electrolyzer. (g) Polarization curves of bifunctional Ni-S-Se/NF for urea electrolysis and water electrolysis.[44] (h) Scheme of the fabrication of Fe-Ni_3S_2 electrode. (i) SEM image of Fe-Ni_3S_2. (j) LSV curves for water electrolysis and urea electrolysis using bifunctional Fe-Ni_3S_2. (k) Stability curves of Fe-Ni_3S_2 for water electrolysis and urea electrolysis.[111]

434 Integrating the merits of multi-components into one catalyst exhibits high efficiency to upgrade

435 the catalytic performance of chalcogenides due to the interfacial synergetic and electronic

436 modulation.   Chalcogenide/carbon,[114]   chalcogenide/metal,[115]   chalcogenide/alloy,[116]

chalcogenide/(hydr)oxide,[117] chalcogenide/phosphide,[118] and chalcogenide/chalcogenide hybrids[119, 120] have been designed for urea electrolysis. Carbon materials (e.g., graphene,[121] MWCNTs,[114] and N-doped carbon[122]) are generally employed to enhance the electronic conductivity and benefit active sites exposure and electron transport of chalcogenide-based catalysts. Interestingly, Zhang et al. found that the interfacial interaction between N-doped carbon and Ni center promotes water dissociation and optimizes H* adsorption/desorption, with a thermo-neutral hydrogen adsorption free energy.[122] In terms of chalcogenide/metal compound heterostructures, most studies focus on the interfacial interaction-regulated electronic properties, and the introduction of additional catalytic active sites. These two effects are account for explaining the enhanced intrinsic activities of chalcogenide/metal compound composites. For a Fe-doped $Co_{0.85}Se$/FeCo LDH composite (Fe-$Co_{0.85}Se$/FeCo LDH) synthesized via a partial selenization treatment (**Fig. 7a**), the formation of interfacial bonding between Fe-$Co_{0.85}Se$ and FeCo LDH results in electron redistribution and regulated electronic structures.[123] Compared with the single phase counterparts, the Fe-doped $Co_{0.85}Se$/FeCo LDH composite exhibits better HER and UOR performance. At 100 mA cm^{-2}, the composite can save 0.16 V for UOR than OER (**Fig. 7b**), suggesting an boosted anodic reaction. Further *in situ* Fourier transform infrared (FTIR) spectra indicate an CNO^{-} intermediate during UOR (**Fig. 7c-d**). DFT calculations disclose that the interface bonding facilitates H adsorption/desorption for HER and promotes urea adsorption/activation/dissociation during UOR (**Fig. 7e-f**).

Among diverse composite catalysts, Mott–Schottky heterojunctions that couple a semiconductor with a metallic component at nanoscale gain great interest. In a Mott–Schottky heterojunction, electrons spontaneously flow across the heterointerface and form a built-in electric field, which redistributes electron cloud densities and forms local electrophilic/nucleophilic regions.[124]

27

Recently, Se/NiSe$_2$,[43] CoS$_2$/MoS$_2$,[30] MoS$_2$/Ni$_3$S$_2$,[125] and NiS/MoS$_2$[126] Mott–Schottky heterojunctions have been fabricated for urea electrolysis. Take the hydrothermally synthesized NiS/MoS$_2$ as an example (**Fig. 7g**), the spontaneous electron transfer from MoS$_2$ to NiS leads to a built-in electric field (**Fig. 7h-j**).[126] The built-in electric field accelerates charge transfer efficiency and modifies adsorption strength for reaction intermediates, ultimately accelerating water and urea molecule dissociation. Together with its hierarchical structure and superior hydrophilicity (**Fig. 7k**), the NiS/MoS$_2$ composite significantly outperforms the NiS and MoS$_2$ analogues for UOR (**Fig. 7l**) and HER.
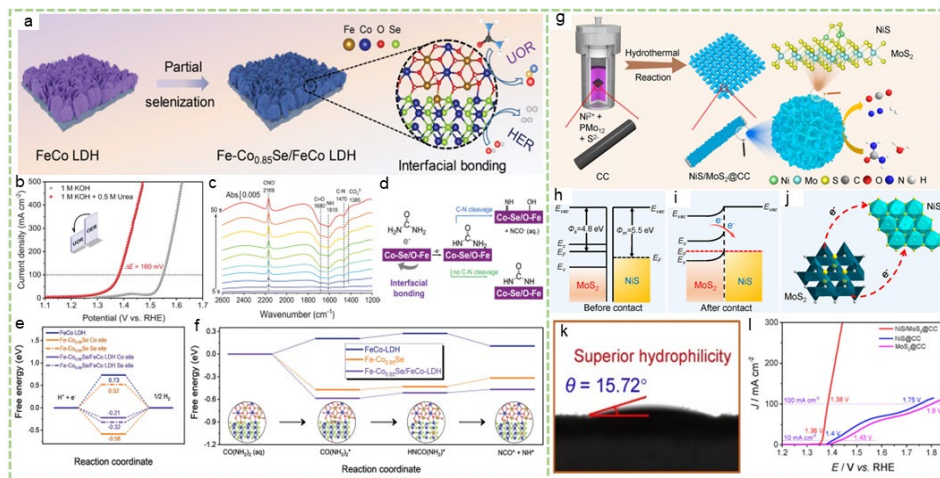
Fig .7 (a) Scheme of the fabrication of Fe-Co$_{0.85}$Se/FeCo LDH. (b) LSV curves of Fe-Co$_{0.85}$Se/FeCo LDH for OER and UOR. (c) Time-dependent FTIR profile of Fe-Co$_{0.85}$Se/FeCo LDH during UOR at 1.45 V vs. RHE. (d) Illustration of possible intermediates in UOR. (e) HER free energy profiles of Fe-Co$_{0.85}$Se/FeCo LDH, Fe-Co$_{0.85}$Se, and FeCo LDH. (f) Simplified UOR free energy profiles of Fe-Co$_{0.85}$Se/FeCo LDH, Fe-Co$_{0.85}$Se, and FeCo LDH.[123] (g) Illustration of the synthesis of NiS/MoS$_2$@CC. (h) and (i) Energy band profiles of MoS$_2$ and metallic NiS before and after contact. (j) Scheme of the charge transfer process between NiS and MoS$_2$. (k) contact angle image of NiS/MoS$_2$@CC. (l) LSV curves of MoS$_2$@CC, NiS@CC, and NiS/MoS$_2$@CC for UOR.[126]

4.5. Metal pnictides

Transitional metal pnictides, i.e., nitrides and phosphides, are well investigated urea electrolysis electrocatalysts for their high electrical conductivity, good redox activity, flexible composition and phase, as well as low cost.[46] Many Ni/Co/Fe-based pnictides exhibit good performance towards both HER and UOR, and researchers have concentrated on design strategies like nanostructure control, chemical composition optimization, heteroatom doping, and heterostructure construction.

High-performance nitrides and phosphides with diverse nanostructures have been developed. Generally, nitrides and phosphides synthesized via direct high-temperature processes show a nanoparticle structure,[127] which bears the drawback of low SSA and thus limited active sites. To address this issue, it is sensible to use hydrothermally synthesized metal oxides/hydroxides and MOFs as the precursor for metal nitrides and phosphides.[46, 128, 129] The two-step synthetic route can obtain nitrides and phosphides with high active area. For example, Liu and coworkers developed Ni_2P nanoflake arrays on carbon cloth from the NiO nanoflake arrays via low-temperature phosphization, and large open spaces between nanoflakes ensure rich active sites are and accelerate electrolyte/gaseous product diffusion during electrochemical reactions.[129]

Compared with binary transition metal pnictides, ternary and quaternary pnictides with two or more metal components exhibit better electrocatalytic performance. Introducing additional metals into pnictides can populate active sites, and regulate the electronic properties of catalysts via intermetallic electron transfer.[130] NiCoP,[131] NiFeP,[132] FeCoP,[133] CoMoN,[130] and NiVMnN[134] are representative bifunctional ternary and quaternary pnictide catalysts for urea electrolysis. Starting from a Ni-Co Prussian blue analogue, Ding et al. designed a hollow NiCoP nanoprism catalyst (**Fig. 8a-c**).[47] Due to the presence of Co, the NiCoP catalyst outperforms Ni_2P for both UOR and

29

HER. As a bifunctional catalyst, NiCoP can attain 100 mA cm^{-2} at 1.57 and 1.77 V for urea

electrolysis and water electrolysis respectively (**Fig. 8d**). Computational results disclose that the

introduction of Co improves the DOS at the Fermi level, boosting water dissociation and hydrogen

evolution steps and enhancing the absorption of water and urea molecules (**Fig. 8e-g**). Similar

enhancement has been found in the CoNi oxyphosphides (CoNiOP) developed with a MOF

precursor (**Fig. 8h**).[135] CoNiOP exhibits better performance than CoOP for urea electrolysis due to

the accelerated *in situ* phase transformation and optimized intermediates adsorption processes

induced by the electrons transfer from bimetal centers to anion at the interface (**Fig. 8i-j**). In the

quaternary NiVMnN, the introduction of Mn^{2+} helps to stabilize high-valence V^{5+} and Ni^{2+} species,

providing stable electroactive sites. The effective electronic transition between Mn and Ni also

contributes to excellent UOR performance.[134] A key issue related to the component regulation is

the rationalization of metal ratios in metal pnictides, which should largely affect the catalytic

performance but little attention has been paid on it.
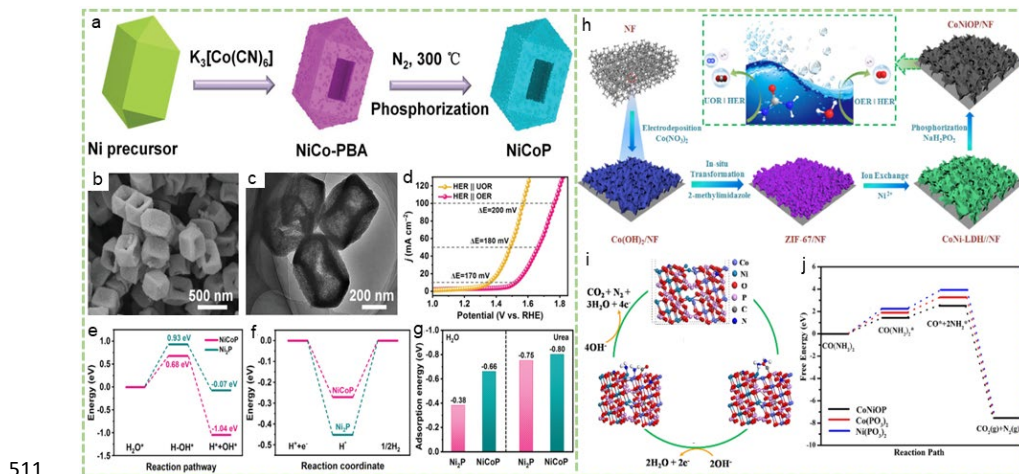
Fig. 8 (a) Diagram of the synthesis of NiCoP. (b) SEM and (C) TEM images of NiCoP. (d) LSV curves of bifunctional NiCoP for water electrolysis and urea elkectrolysis. Energy profiles for (e) water dissociation, (f) hydrogen evolution, and (g) urea and water adsorption over NiCoP and Ni_2P.[47] (h) Scheme of the preparation of CoNiOP. (i) DFT calculation models of UOR reactions over CoNiOP. (j) Free energy diagrams of UOR over of CoNiOP.[135]

Doping metal pnictides with metals or nonmetals allows to regulate the electronic properties of catalysts, thereby enhancing the catalytic performance. For example, introducing Co into the Ni-P-O catalyst decreases the conversion potential of Ni^{2+}/Ni^{3+} and the UOR onset potential; for HER, the Co dopant enhances the water dissociation ability of $Ni(OH)_2$ and the hydrogen desorption process of NiP.[136] For the V-doped Ni_3N,[137] Ru-doped Ni_3N,[138] and Mo, Fe co-doped Co_2P[48], dopants have been evidenced to regulate the adsorption of reaction intermediates and lead to near zero Gibbs free energy. Aside from most metal-doped pnictides, oxygen-incorporated NiMoP developed by Jiang et al. shows upgraded performance for urea electrolysis.[139] Although oxygen does not act as the active site, the presence of oxygen modulates the electronic environment of Ni site, facilitates water dissociation for HER, and optimizes intermediate adsorption/desorption for UOR.

Metal pnictide/carbon composites are developed to enhance the performance of catalysts. Incorporating 2D graphene is suggested to improve the conductivity of pnictide catalysts.[140-142] Differently, carbon materials may also contribute to the intrinsic activity and stability of catalysts. For the carbon coated NiCoP with a sea urchin-like nanostructure, the carbon layer promotes the charge transfer efficiency and structural stability of catalyst.[143] Xiao et al. suggested that the N-doped carbon layer on Ni_2P nanoparticles not only boosted the electrical conductivity and long-term stability but also improved electrolyte/gaseous transport by maintaining a peapod-like nanostructure.[144] In the 2D CoP/carbon particle composite, the inserted carbon particles increase

the catalytic performance by exposing more electroactive sites, improving contact area between electrolyte and catalyst active surface, and accelerating the mass/electron transfer efficiency in urea electrolysis.[145]

Hybridizing metal pnictides with other electroactive components is effective in attaining high-performance catalysts. Metals,[146] oxides,[147] hydroxides,[148] sulfides[149, 150] and pnictides[151, 152] have been employed to regulate the properties of metal pnictides. These metal pnictide-based heterostructures share the common feature of enlarged active surface area and enhanced intrinsic activities due to the interface interaction between pnictides and the other active components. For instance, the Mo particles/Ni-P matrix (Mo/Ni-P) synthesized by electrodeposition (**Fig. 9a**) combines the merits of both multi-valence Mo and NiP species for efficient urea electrolysis.[153] At 1.55 V, the bifunctional Mo/Ni-P can attain 50 mA cm^{-2}, with a high stability for 12 h at 100 mA cm^{-2} (**Fig. 9b-d**). Furthermore, the Mo/Ni-P involved urea electrolysis process successfully works in a solar-H$_2$-electricity conversion system, and the electric fan is driven by the solar-hydrogen conversion device (**Fig. 9e**). In another Ni/W$_5$N$_4$ Mott-Schottky heterojunction, the charge transfer at the interface is considered a main reason for explaining its high catalytic performance towards urea electrolysis (E_{10} = 1.33 V).[146] For some Ni/Co-free pnictides which has good HER performance, it is necessary to introduce a Ni/Co-based components to enhance their UOR activities. Wang and co-authors developed a MoP@NiCo-LDH composite via a hydrothermal process-phosphorization-electrodeposition method (**Fig. 9f**).[154] Compared with MoP and NiCo-LDH, the composite exhibits better performance for both HER and UOR. It is found that the NiCo hydroxide can effectively adsorb OH groups and accelerate water dissociation for HER, and the in situ generated NiCo oxyhydroxide phase boosts the UOR performance. For overall urea electrolysis, a lower potential (~1.4 V) is required for MoP@NiCo-LDH to achieve 100 mA cm^{-2}

than its counterparts (**Fig. 9g-h**). The out-layer LDH also benefits the stability of catalyst, and a stable current density is recorded for 20 h; also, the composite has good structural stability (**Fig. 9i-j**). Following such a modular design principle, NiP$_2$/ZnP$_4$[155] and Ni$_3$N/Mo$_2$N[151] have also been innovated for urea electrolysis.
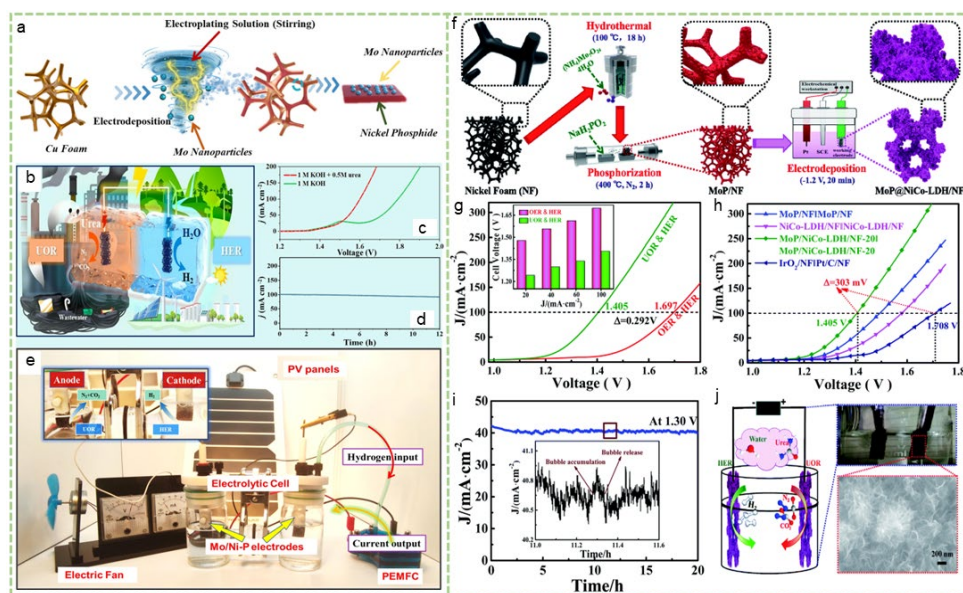
Fig. 9 (a) Scheme of the synthesis of Mo/Ni-P. (b) Illustration of the urea electrolysis system. (c) LSV curves of bifunctional Mo/Ni-P for urea electrolysis and water electrolysis. (d) Stability curve of Mo/Ni-P for urea electrolysis. (e) Image of the solar-H$_2$-electricity energy conversion device.[153] (f) Illustration of the preparation of MoP@NiCo-LDH. (g) LSV curves of bifunctional MoP@NiCo-LDH for water electrolysis and urea electrolysis. (h) LSV curves of bifunctional MoP@NiCo-LDH, MoP, NiCo-LDH, and IrO$_2$||Pt/C couple for urea electrolysis. (i) I-t curve of MoP@NiCo-LDH at 1.30 V for urea electrolysis. (j) Image of MoP@NiCo-LDH/NF as electrodes for urea electrolysis and SEM image of MoP@NiCo-LDH/NF after 20 h stability test.[154]

4.6. SACs, MOFs, and others

SACs emerge as effective catalysts for diverse applications, due to their ultrahigh atomic utilization efficiency. In SACs, highly isolated metal-atoms (in most cases) are anchored on substrates with a large SSA. The coordination environment of SACs governs the catalytic performance, and thus it is important to design suitable substrates for the central single metal atoms. For example, loading Pt single atoms onto defective NiCo LDH (Pt/D-NiCo LDH) is proved to be an efficient method to develop a bifunctional catalyst for urea electrolysis.[156] With a hierarchical architecture, rich single Pt atomic sites, and abundant edge sites, the Pt/D-NiCo LDH catalyst can catalyze urea electrolysis at 1.32 V for 10 mA cm^{-2}. Similarly, NiV LDH has been used to support Rh SACs (Rh/NiV-LDH) by a hydrothermal method (**Fig. 10a**).[34] The Rh/NiV-LDH catalyst composes of densely interconnected nanosheets (**Fig. 10b**), which can provide rich ECSA and accelerate mass/charge transfer during electrochemical tractions. In addition, the aberration-corrected high-angle annular dark-field scanning TEM (AC-HAADF-STEM) images display rich and highly dispersed Rh dots with significant contrast on the LDH support (**Fig. 10c-d**). Compared with Ni(OH)$_2$ and NiV LDH, the Rh/NiV-LDH exhibits much better performance towards urea electrolysis (E_{100} = 1.47 V, F**ig. 10e**), and the urea electrolysis significantly realizes urea removal with high stability for 3 cycles (**Fig. 10f**). Mechanism study reveals that Rh/NiV-LDH possesses a higher d-band center than NiV-LDH (−3.432 vs. −3.685 eV), thereby higher interactions with reaction intermediates. The hydrogen adsorption free energy (ΔG_{H*}) and UOR energy profiles further emphasize the critical role of Rh sites in the adsorption/activation of HER and UOR intermediates (**Fig. 10g-h**). Both reported Pt and Rh-based SACs show good performance but utilize noble metals, and further work may develop Ni or other low-cost metals-based SACs for urea electrolysis.

593
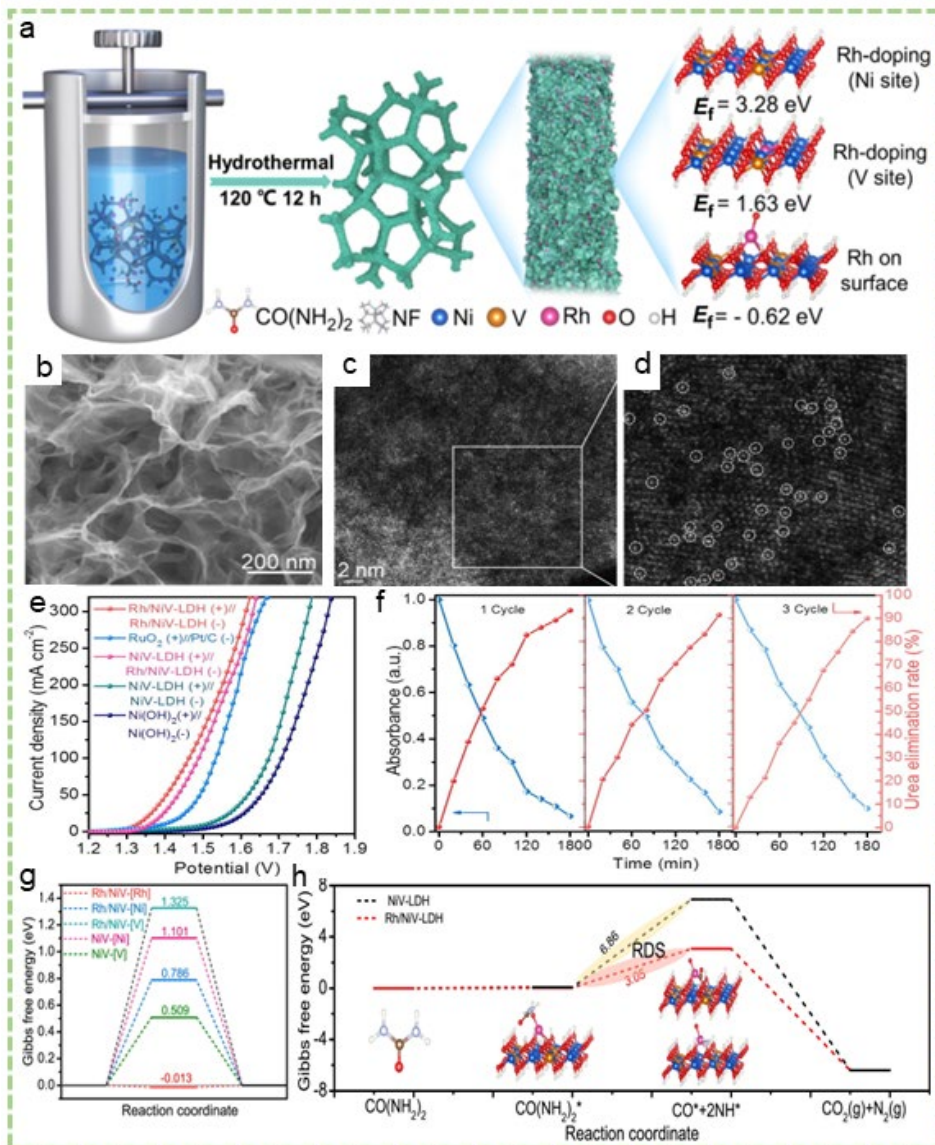
Fig. 10 (a) Schematic of the fabrication of Rh/NiV-LDH. (b) SEM image of Rh/NiV-LDH. (c, d) Aberration-corrected

STEM images of Rh/NiV-LDH. (e) LSV curves of Rh/NiV-LDH and its counterparts for urea electrolysis. (f) Urea

elimination efficiency and recyclability performance. (g) Calculated ΔG_{H*} on possible sites over Rh/NiV-LDH and

NiV-LDH. (h) UOR free energy dirgram over Rh/NiV-LDH and NiV-LDH.[34]

Besides being used as precursors for designing metal-based catalysts, MOFs can be directly used as electrocatalysts for urea electrolysis owing to their highly porous feature and flexible composition. For example, the nickel terephthalate nanosheets self-assembled 3D aggregates, with rich unsaturated coordination nickel sites, take 1.52 V at 10 mA cm^{-2} for urea electrolysis.[12] The performance of single metal-based MOFs can be enhanced by introducing a second metal. With a hydrothermal method, Zhang et al. developed a Fe-doped Ni-MOF catalyst which is composed of interconnected vertical nanosheets (**Fig. 11a-b**).[51] Compared with bare Ni-MOF, the introduction of Fe generates some new electronic states near the Fermi level and thus activates the Ni active sites (**Fig. 11c-e**). As evidenced by the adsorption energies of H_2O, N_2, and urea molecules, the Fe-doped Ni-MOF favours the adsorption of H_2O and urea molecules and the desorption of N_2 (**Fig. 11f**), contributing to enhanced UOR performance. Also, Fe-doped Ni-MOF shows a significantly lower charge transfer resistance than Ni-MOF, indicating an efficient charge transport process (**Fig. 11g**). For urea electrolysis, Fe-doped Ni-MOF can save 0.3 V at 50 mA cm^{-2} than for water electrolysis (**Fig. 11h**). Besides heteroatom doping, combining MOFs with other active and conductive components has also been investigated. Benefiting from the multicomponent synergistic effect, urchin-like CoS$_x$/Co-MOF,[50] Ni$_2$P@Ni-MOF,[157] NiCoP$_x$@NiFeCo-MOF,[158] and Ru-modified NiFe MOF[159] possess high-performance for urea electrolysis. In these composites, the hierarchical MOF framework can host the additional active species and lead to rich active sites and regulated electronic properties for enhanced performance.
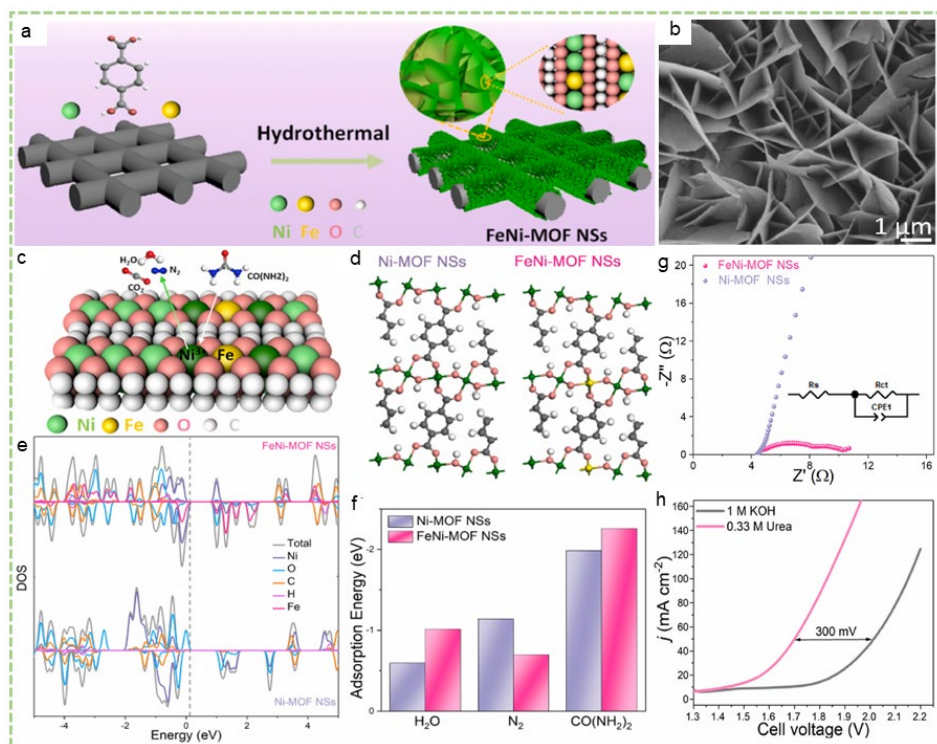
Fig. 11 (a) Scheme of the synthesis of FeNi-MOF nanosheet arrays (NSs). (b) SEM image of FeNi-MOF NSs. (c) Illustration of the UOR process over FeNi-MOF NSs. (d) Optimized (101) surface models of Ni-MOF NSs and FeNi-MOF NSs. (e) DOS for (101) surfaces of Ni-MOF NSs and FeNi-MOF NSs. (f) Adsorption free energy of N_2, $CO(NH_2)_2$, and H_2O on the (101) surfaces of Ni-MOF NSs and FeNi-MOF NSs. (g) LSV curves of FeNi-MOF NSs for OER, UOR, and HER. (h) LSV curves of bifunctional FeNi-MOF NSs for urea electrolysis and water electrolysis.[51]

A small group of other metal-based catalysts, like carbides,[160, 161] fluoride,[53, 162] and borides[52] have been investigated for urea electrolysis. A main feature of these catalysts is their high conductivity and activity. The development of these types of catalysts for urea electrolysis is still poorly explored, and some key points need to be considered. For carbides usually fabricated via high-temperature processes, it is necessary to introduce a conductive substrate (e.g., graphene, CNTs,

628   N-doped carbon) with large SSA to attain rich active sites. The design, synthesis, and application

629   of metal fluorides should take the negative environmental effect of F element into consideration.

630   In terms of borides which can be simply prepared by electroless deposition, it is crucial to enhance

631   their performance via chemical composition optimization and composite construction.

632   5. Benchmarking bifunctional electrocatalysts for practical applications

633   In the past few years, great progress has been achieved in bifunctional catalysts for urea electrolysis.

634   Catalysts with different compositions and nanostructures are showcased in the last section. To

635   further guide the design of high-performance catalysts, it is important to evaluate the catalytic

636   performance of current catalysts in an accurate and objective manner. Currently, E_{10} is the most

637   widely used indicator of bifunctional catalysts' activity, with a group of studies applied E_{20}, E_{50},

638   E_{100}, or E_{500} (**Table S1**, Supporting Information). Another issue related to the performance

639   evaluation is the property of electrolytes, and electrolytes with diverse urea concentrations lead to

640   distinct performance for one catalyst.[89, 163] 1 M KOH with 0.33 M urea or 0.5 M urea is the most

641   widely used electrolyte, and several studies also employed 0.1 M, 0.2 M, 0.3 M or 0.4 M urea. In

642   this context, the E_{10} values of catalysts measured in 1 M KOH + 0.33 M urea (56 studies, 1 M

643   KOH + 0.3 M urea is included) or 1 M KOH + 0.5 M urea (70 studies) are compared separately.

644   As depicted in **Fig. 12**, E_{10} values mainly range from 1.3 to 1.6 V, in both electrolyte conditions.

645   The best value (1.26 V) tested in 1 M KOH + 0.33 M urea is obtained by N-doped $FePS_3$, while

646   the CoS_2/MoS_2 composite shows the best performance (E_{10} = 1.29 V) in 1 M KOH + 0.5 M urea.

647   In the 1 M KOH + 0.33 M urea system, 37.5% of all catalysts show E_{10} values less than 1.4 V,

648   which is similar to this percentage (40%) in the 1 M KOH + 0.5 M urea electrolyte. It should be

649   noted that deviations of electrochemical measurements (e.g., testing temperature, catalyst loading

650 amount, LSV scanning rate, and electrode fabrication method) would affect the recorded activity.

651 Hence, the comparison made here may not be accurate enough, and we suggest potential readers

652 be fully aware of this.

653 The urea electrolysis performance of five novel metal-involved catalysts has been tested in 1 M

654 KOH + 0.33 M urea, including Pt/D-NiCo LDH (1.32 V),[156] P modified AuRh (1.33 V),[56] Rh/NiV-

655 LDH (1.336 V),[34] NiFeRh-LDH (1.35 V),[89] and Ru-Ni$_3$N@NC (1.41 V)[138]. In these catalysts, the

656 presence of noble metals can enhance the catalytic performance. Especially, using noble metals as

657 dopants and SACs can improve their utilization efficiency and limit the fabrication cost of catalysts.

658 Compared with earth-abundant transition metal-based catalysts, there is no clear advantage in the

659 performance of noble metal-based catalysts, and thus most studies focus on low-cost transition

660 metals, especially Ni.
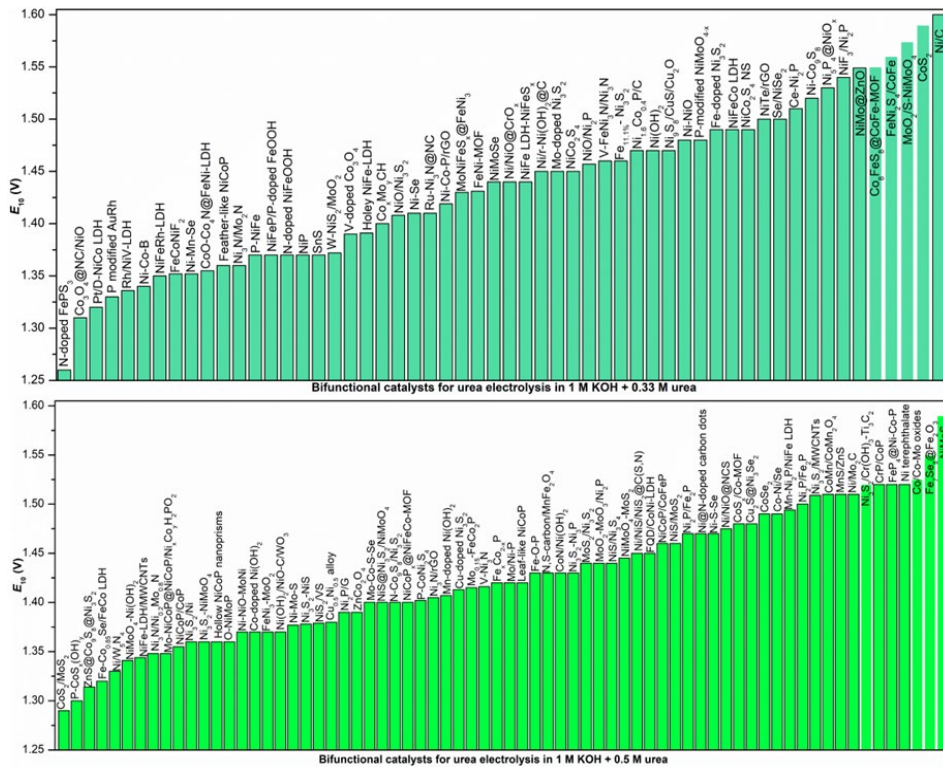
Fig. 12 A comparison of bifunctional catalysts for urea electrolysis in different electrolytes.

Further identify high-performance catalysts, E_{10} of ten most promising electrocatalysts in both electrolyte systems are analyzed (**Table 2**). It can be seen that most of the listed high-performance catalysts possess open architectures with large SSA, which can not only promote electrolyte diffusion/penetration/infiltration but also and facilitate charge transfer and mass (ions, reaction intermediates, gaseous products) transport. In terms of the chemical composition, transition metal-based LDHs with typical 2D nanosheet structure attract great interest, and a series of LDH-based composites exhibit excellent catalytic activities for urea electrolysis. Other transition metal-based highly conductive heterostructures are highly promising catalysts, such as sulfides, phosphides,

40

671 and nitrides. Several heteroatom doped catalysts also show high activities, indicating the feasibility

672 of heteroatom doping in regulating the intrinsic activity of catalysts. These results imply that

673 efficient catalysts for urea electrolysis should meet the multiple requirements of high intrinsic

674 activity, large active area, and efficient mass/charge transfer.

675 **Table 2**. List of representative bifunctional electrocatalysts in their ascending values, in both 1 M KOH + 0.33 M urea

676 and 1 M KOH + 0.5 M urea systems.

Catalyst	Electrolyte	E_{10}	Key features
N-doped FePS$_3$[110]	1 M KOH +0.33 M urea	1.26	2D nanosheet structure, N dopant activates intrinsic activity
Co$_3$O$_4$@NC/NiO[77]	1 M KOH +0.3 M urea	1.31	MOF-derived hierarchical composite, synergistic effect between the metal oxide–NC–metal oxide
Pt/D-NiCo LDH[156]	1 M KOH +0.33 M urea	1.32	Noble metal SAC on defective LDH nanosheets
P modified AuRh[56]	1 M KOH +0.33 M urea	1.33	Mesoporous noble metal alloy film, surface chemical modification
Rh/NiV-LDH[34]	1 M KOH +0.33 M urea	1.336	Noble metal SAC on ultrathin LDH nanosheets
Ni-Co-B[52]	1 M KOH +0.33 M urea	1.34	Porous and amorphous metallic structure
NiFeRh-LDH[89]	1 M KOH +0.33 M urea	1.35	Noble metal-doped ultrathin LDH interconnected nanosheets
FeCoNiF$_2$[162]	1 M KOH +0.33 M urea	1.352	Hollow nanoflake arrays, electron-deficient metal centers
Ni–Mn–Se[113]	1 M KOH +0.33 M urea	1.352	Nano-micro hollow spheres, porous structure
CoO–Co$_4$N@NiFe-LDH[148]	1 M KOH +0.33 M urea	1.355	Hierarchical heterostructure, LDH/oxide/nitride composite

41

CoS_2/MoS_2[30]	1 M KOH +0.5 M urea	1.29	Schottky heterojunction, spatially interconnected nanoplates
$P-CoS_x(OH)_y$[109]	1 M KOH +0.5 M urea	1.3	Porous and amorphous core–shell nanoneedles, surface chemical modification
$ZnS@Co_9S_8@Ni_3S_2$[164]	1 M KOH +0.5 M urea	1.314	MOF-derived hollow nanosword arrays, tricomponent sulfide composite
$Fe-Co_{0.85}Se/FeCo\ LDH$[123]	1 M KOH +0.5 M urea	1.32	hierarchical arrays, LDH/selenide composite
Ni/W_5N_4[146]	1 M KOH +0.5 M urea	1.33	Schottky heterojunction, nano-microspheres
$NiMoO_4–Ni(OH)_2$[10]	1 M KOH +0.5 M urea	1.341	3D interconnected pore-like structure, LDH/oxide composite
$NiFe-LDH/MWCNTs$[91]	1 M KOH +0.5 M urea	1.344	Gracile nanosheet arrays, LDH/carbon composite
$Ni_3N/Ni_{0.2}Mo_{0.8}N$[49]	1 M KOH +0.5 M urea	1.348	Hierarchical nanorod arrays, nitride/nitride composite
$Mo-NiCoP@NiCoP/Ni_XCo_YH_2PO_2$[165]	1 M KOH +0.5 M urea	1.348	3D branched core/shell nanorod heterostructure, phosphide/phosphate composite, metal-doping
$NiCoP/CoP$[152]	1 M KOH +0.5 M urea	1.355	Hierarchical heterostructure, phosphide/phosphide composite

677 To meet the potential industrial application of catalysts for urea electrolysis, it is necessary to

678 record the activity at high current densities. To date, 30 studies have provided E_{100} values of

679 catalysts and two studies further test E_{500} values, as shown in **Fig. 13**. E_{100} values mainly range

680 from 1.4 to 1.7 V, and most of the catalysts (oxides, phosphides, sulfides, nitrides, LDH, etc.) are

681 fabricated from low-cost elements, with two noble metal-doped materials (Ru-modified NiFe

682 MOF,[159] Ru-doped Co_2P/N-doped carbon[166]). In addition, the E_{500} values of $Ni_3S_2–NiMoO_4$,

42

683    $Ni_{12}P_5$/Ni-Pi, and Ru/P dual-doped $NiMoO_4$ are 1.61, 1.662 and 1.73 V, respectively. These reports

684   indicate the promising application of cost-effective catalysts in industrial urea electrolyzers.
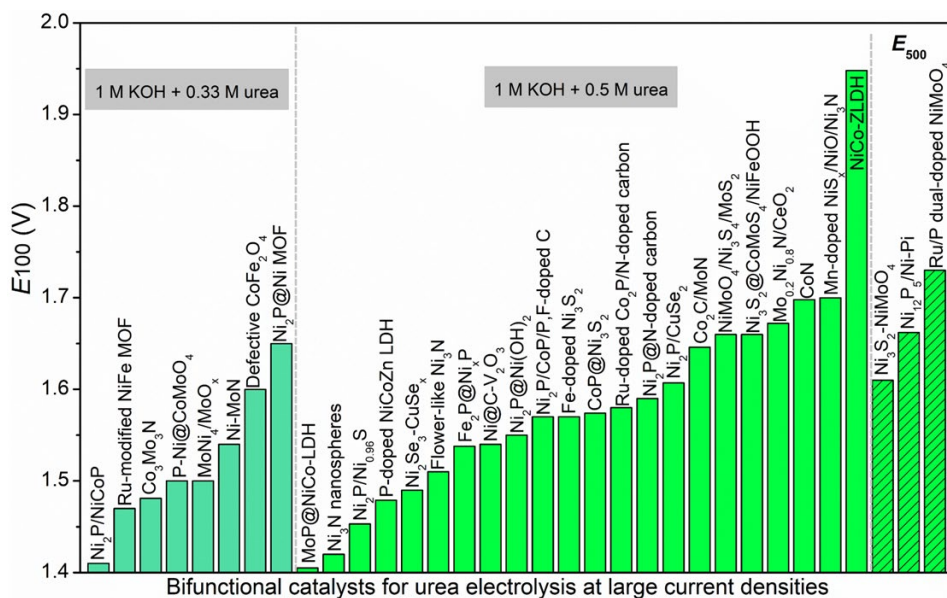
Fig. 13 A comparison of bifunctional catalysts for urea electrolysis at large current densities.

6. Conclusion and perspectives

688   In this review, recent progresses and achievements in the design of bifunctional catalysts for urea

689   electrolysis are comprehensively analyzed. Transition metal (mainly Ni, Co, Fe)-based materials

690   with diverse compositions and nanostructures have exhibited good performance towards both HER

691   and UOR, showing good potential for future industrial applications. For achieving high-

692   performance bifunctional catalysts, powerful strategies have been rationally applied, such as

693   heteroatom doping, composition optimization, heterostructure construction, nanostructure control,

694   defect/vacancy introduction, and phase regulation. Notwithstanding astonishing advances in

695   bifunctional catalysts design, there are some critical issues that require further investigation.

696   1) *Qualitative and quantitative analysis of urea oxidation products*. In most cases, researchers

697   only take CO_2, N_2, and H_2O as urea oxidation products. However, recent studies have shown

698   that other nitrogen-based components are generated during UOR, such as NO_3^- and NO_2^-.[9]

699   The formation of such NO_x^- would lead to secondary pollutants in water bodies. In this context,

700   it is highly urgent to obtain qualitative and quantitative results of urea oxidation products,

701   which can help to uncover the UOR mechanism. Since the urea oxidation pathway is highly

702   sensitive to the applied electrocatalysts, it is possible to selectively limit the production of

703   hazardous NO_x^- and make the urea electrolysis process more eco-friendly.

704   2) *Electrolysis mechanism understanding with advanced tools*. Many studies mainly focus on the

705   performance of catalysts, while the urea electrolysis mechanism is still far from fully

706   understood. Apart from the quantitative analysis of urea oxidation products, it is needed to

707   figure out the structure-performance relationship of catalysts with advanced techniques, like

708   ion chromatography, gas chromatography, *in situ* Raman spectra, *in situ* XAS spectra, *in situ*

709   FTIR spectra. The related *in situ* tools are highly recommended to capture the reaction

710   intermediates during the complex UOR process. Another key issue is the self-reconstruction

711   of catalysts during HER and UOR. The self-reconstruction process leads to the formation of

712   real active phases and can be determined by *in situ* Raman spectra. When conducting DFT

713   calculations, it is suggested to take the catalyst self-reconstruction into account for reaction

714   model construction.

715   3) *Large-scale fabrication of electrocatalysts/electrodes*. For the industrial application of

716   promising catalysts, it is necessary to develop large-scale catalyst/electrode fabrication

44

techniques. Due to the high activity of Ni for both HER and UOR, many studies directly use nickel foam as the support to construct active materials. Also, some conductive materials also have been used as the substrate of active materials, e.g., Fe foam, Cu foam, Ti mesh, carbon papers and carbon cloth. These self-supported electrodes are generally prepared with a small geometric area, for laboratory use. The large-scale of such self-supported electrodes needs large synthetic devices (such as hydrothermal autoclave reactors). For binder-based electrodes, the large-scale production of powder-like active materials can be achieved by using more facile methods, like high-energy ball milling.

4) *Application of catalysts in real urea wastewater electrolysis*. Instead of pure alkalized urea solutions, it is suggested to perform urea-rich wastewater (e.g., urine) electrolysis for hydrogen fuel production and urea degradation. In real wastewater, there will be diverse inorganic and organic pollutants which may influence the urea electrolysis efficiency. Several studies have conducted real urine electrolysis, and the experimental results suggest that catalysts work worse in alkalized urine solution than in pure alkalized urea solution,[37, 167-169] while the reason remains unclear. As such, future studies are suggested to identify pollutants in real urea-rich electrolytes and analyze the effect of potential substances on the urea electrolysis. A further step to lower the energy cost of urea electrolysis can be achieved by integrating solar energy into the electrolysis system.

Author contributions

Zhijie Chen: conceptualization, writing-original draft; **Wei Wei**: data analysis, writing-review & editing; **Bing-Jie Ni**: discussions, writing-review & editing, project acquisition.

Conflict of Interest

The authors declare no conflict of interest.

References

> **Commented [H1]:** Please cite more references published in the last two years.

1. X. Zhang, X. Zhu, S. Bo, C. Chen, M. Qiu, X. Wei, N. He, C. Xie, W. Chen, J. Zheng, P. Chen, S. P. Jiang, Y. Li, Q. Liu and S. Wang, *Nature Communications*, 2022, **13**, 5337.
2. J. Li, S. Wang, S. Sun, X. Wu, B. Zhang and L. Feng, *Journal of Materials Chemistry A*, 2022, **10**, 9308-9326.
3. W. Sun, M. Zhang, J. Li and C. Peng, *ChemSusChem*, 2022, **15**, e202201263.
4. G. Wang, Y. Ling, X. Lu, H. Wang, F. Qian, Y. Tong and Y. Li, *Energy & Environmental Science*, 2012, **5**, 8215-8219.
5. Q. He, Y. Wan, H. Jiang, Z. Pan, C. Wu, M. Wang, X. Wu, B. Ye, P. M. Ajayan and L. Song, *ACS Energy Letters*, 2018, **3**, 1373-1380.
6. L. Wang, Y. Zhu, Y. Wen, S. Li, C. Cui, F. Ni, Y. Liu, H. Lin, Y. Li, H. Peng and B. Zhang, *Angew Chem Int Ed Engl*, 2021, **60**, 10577-10582.
7. J.-Y. Zhang, T. He, M. Wang, R. Qi, Y. Yan, Z. Dong, H. Liu, H. Wang and B. Y. Xia, *Nano Energy*, 2019, **60**, 894-902.
8. Z. Ji, Y. Song, S. Zhao, Y. Li, J. Liu and W. Hu, *ACS Catalysis*, 2021, DOI: 10.1021/acscatal.1c05190, 569-579.
9. X. Liu, H. Qin, G. Wang, Q. Li, Q. Huang, Z. Wen and S. Mao, *Journal of Materials Chemistry A*, 2022, **10**, 16825-16833.
10. S. Hu, H. Wu, C. Feng and Y. Ding, *International Journal of Hydrogen Energy*, 2020, **45**, 21040-21050.
11. Q. Zhang, M. Sun, J. Zhu, S. Yang, L. Chen, X. Yang, P. Wang, K. Li, F. Xue, Y. Lu, J. Zhang and P. Zhao, *Chemical Engineering Journal*, 2022, **432**, 134275.
12. S. Zheng, Y. Zheng, H. Xue and H. Pang, *Chemical Engineering Journal*, 2020, **395**, 125166.
13. X. Wang, J. P. Li, Y. Duan, J. Li, H. Wang, X. Yang and M. Gong, *ChemCatChem*, 2022, **14**.
14. Y. Ma, C. Ma, Y. Wang and K. Wang, *Catalysts*, 2022, **12**.
15. B. Zhu, Z. Liang and R. Zou, *Small*, 2020, **16**, e1906133.
16. X. Sun and R. Ding, *Catalysis Science & Technology*, 2020, **10**, 1567-1581.
17. X. Hu, J. Zhu, J. Li and Q. Wu, *ChemElectroChem*, 2020, **7**, 3211-3228.
18. G. Gnana kumar, A. Farithkhan and A. Manthiram, *Advanced Energy and Sustainability Research*, 2020, **1**.
19. W. Xu, Z. Wu and S. Tao, *Energy Technology*, 2016, **4**, 1329-1337.
20. R. K. Singh, K. Rajavelu, M. Montag and A. Schechter, *Energy Technology*, 2021, **9**, 2100017.
21. W. Ge, L. Lin, S.-Q. Wang, Y. Wang, X. Ma, Q. An and L. Zhao, *Journal of Materials Chemistry A*, 2023.
22. L. Fei, H. Sun, X. Xu, Y. Li, R. Ran, W. Zhou and Z. Shao, *Chemical Engineering Journal*, 2023, 144660.

46

780   23.   J. Ge, J. Kuang, Y. Xiao, M. Guan and C. Yang, *Surfaces and Interfaces*, 2023, 103230.

781   24.   K. Fan, H. Zou, N. A. Dharanipragada, L. Fan, A. K. Inge, L. Duan, B. Zhang and L. Sun, *Journal*
782   *of Materials Chemistry A*, 2021, **9**, 11359-11369.

783   25.   S. Anantharaj, S. Noda, V. R. Jothi, S. Yi, M. Driess and P. W. Menezes, *Angewandte Chemie*
784   *International Edition*, 2021, **60**, 18981-19006.

785   26.   Z. Chen, W. Wei and B.-J. Ni, *Current Opinion in Electrochemistry*, 2021, DOI:
786   10.1016/j.coelec.2021.100888.

787   27.   L. Zhang, L. Wang, H. Lin, Y. Liu, J. Ye, Y. Wen, A. Chen, L. Wang, F. Ni, Z. Zhou, S. Sun, Y. Li,
788   B. Zhang and H. Peng, *Angew Chem Int Ed Engl*, 2019, **58**, 16820-16825.

789   28.   S. Wang, W. Chen, L. Xu, X. Zhu, Y. C. Huang, W. Zhou, D. Wang, Y. Zhou, S. Du, Q. Li, C. Xie,
790   L. Tao, C. L. Dong, J. Liu, Y. Wang, R. Chen, H. Su, C. Chen, Y. Zou, Y. Li and Q. Liu, *Angew*
791   *Chem Int Ed Engl*, 2020, DOI: 10.1002/anie.202015773.

792   29.   P. Wang, X. Bai, H. Jin, X. Gao, K. Davey, Y. Zheng, Y. Jiao and S.-Z. Qiao, *Advanced Functional*
793   *Materials*, 2023, **33**, 2300687.

794   30.   C. Li, Y. Liu, Z. Zhuo, H. Ju, D. Li, Y. Guo, X. Wu, H. Li and T. Zhai, *Advanced Energy Materials*,
795   2018, **8**.

796   31.   Z. Chen, R. Zheng, H. Zou, R. Wang, C. Huang, W. Dai, W. Wei, L. Duan, B.-J. Ni and H. Chen,
797   *Chemical Engineering Journal*, 2023, 142684.

798   32.   Y. Pan, J. Zhang, Q. Zhang, X. Chen, Q. Wang, C. Li, Z. Liu and Q. Sun, *Materials Chemistry*
799   *Frontiers*, 2023, DOI: 10.1039/D2QM01290A.

800   33.   Q. Xu, G. Qian, S. Yin, C. Yu, W. Chen, T. Yu, L. Luo, Y. Xia and P. Tsiakaras, *ACS Sustainable*
801   *Chemistry & Engineering*, 2020, **8**, 7174-7181.

802   34.   H. Sun, L. Li, H.-C. Chen, D. Duan, M. Humayun, Y. Qiu, X. Zhang, X. Ao, Y. Wu, Y. Pang, K.
803   Huo, C. Wang and Y. Xiong, *Science Bulletin*, 2022, **67**, 1763-1775.

804   35.   L. Guo, J. Chi, J. Zhu, T. Cui, J. Lai and L. Wang, *Applied Catalysis B: Environmental*, 2023, **320**,
805   121977.

806   36.   X. Zhuo, W. Jiang, T. Yu, G. Qian, J. Chen, H. Yang and S. Yin, *ACS Applied Materials & Interfaces*,
807   2022, **14**, 46481-46490.

808   37.   D. Wen, W. Peng, W. Zhang, Y. Xia, M. Ye and W. Hu, *Applied Surface Science*, 2023, **608**, 155166.

809   38.   C. B. Sun, M. W. Guo, S. S. Siwal and Q. B. Zhang, *Journal of Catalysis*, 2020, **381**, 454-461.

810   39.   Y. Cheng, F. Liao, H. Dong, H. Wei, H. Geng and M. Shao, *Journal of Power Sources*, 2020, **480**,
811   229151.

812   40.   Z. Yang, Y. Zhang, C. Feng, H. Wu, Y. Ding and H. Mei, *International Journal of Hydrogen Energy*,
813   2021, **46**, 25321-25331.

814   41.   W. Zhu, M. Ren, N. Hu, W. Zhang, Z. Luo, R. Wang, J. Wang, L. Huang, Y. Suo and J. Wang, *ACS*
815   *Sustainable Chemistry & Engineering*, 2018, **6**, 5011-5020.

816   42.   C. Liu, F. Li, S. Xue, H. Lin, Y. Sun, J. Cao and S. Chen, *ACS Applied Energy Materials*, 2022, **5**,
817   1183-1192.

818   43.   S. Khatun and P. Roy, *Journal of Colloid and Interface Science*, 2023, **630**, 844-854.

819   44.   N. Chen, Y.-X. Du, G. Zhang, W.-T. Lu and F.-F. Cao, *Nano Energy*, 2021, **81**.

820   45.   W. Mai, Q. Cui, Z. Zhang, D. Wen, L. Tian and W. Hu, *International Journal of Hydrogen Energy*,
821   2021, **46**, 24078-24093.

822   46.   S. Hu, S. Wang, C. Feng, H. Wu, J. Zhang and H. Mei, *ACS Sustainable Chemistry & Engineering*,
823   2020, **8**, 7414-7422.

824   47.   X. Ding, L. Pei, Y. Huang, D. Chen and Z. Xie, *Small*, 2022, **18**, 2205547.

825   48.   Y. Wang, X. Li, X. Du and X. Zhang, *International Journal of Hydrogen Energy*, 2023, DOI:
826   https://doi.org/10.1016/j.ijhydene.2023.06.240.

827   49.   R.-Q. Li, X.-Y. Wan, B.-L. Chen, R.-Y. Cao, Q.-H. Ji, J. Deng, K.-G. Qu, X.-B. Wang and Y.-C.
828   Zhu, *Chemical Engineering Journal*, 2021, **409**, 128240.

829   50.   H. Xu, K. Ye, K. Zhu, J. Yin, J. Yan, G. Wang and D. Cao, *Inorganic Chemistry Frontiers*, 2020, **7**,
830   2602-2610.

831 51. X. Zhang, X. Fang, K. Zhu, W. Yuan, T. Jiang, H. Xue and J. Tian, *Journal of Power Sources*, 2022,
832 **520**, 230882.
833 52. B. Kim, G. Das, J. Kim, H. H. Yoon and D. H. Lee, *Journal of Colloid and Interface Science*, 2021,
834 **601**, 317-325.
835 53. K. Wang, W. Huang, Q. Cao, Y. Zhao, X. Sun, R. Ding, W. Lin, E. Liu and P. Gao, *Chemical*
836 *Engineering Journal*, 2022, **427**, 130865.
837 54. Z. Chen, W. Wei, L. Song and B.-J. Ni, *Sustainable Horizons*, 2022, **1**.
838 55. L. Wang, L. Ren, X. Wang, X. Feng, J. Zhou and B. Wang, *ACS Applied Materials & Interfaces*,
839 2018, **10**, 4750-4756.
840 56. M. Zhang, Z. Duan, L. Cui, H. Yu, Z. Wang, Y. Xu, X. Li, L. Wang and H. Wang, *Journal of*
841 *Materials Chemistry A*, 2022, **10**, 3086-3092.
842 57. K. Zhang, S. Wang, X. Li, H. Li and Y. Ni, *Small*, 2023, **19**, 2300959.
843 58. J. Zhang, F. Xing, H. Zhang and Y. Huang, *Dalton Transactions*, 2020, **49**, 13962-13969.
844 59. N. Muthuchamy, S. Jang, J. C. Park, S. Park and K. H. Park, *ACS Sustainable Chemistry &*
845 *Engineering*, 2019, **7**, 15526-15536.
846 60. R. Ma, Y. Zhou, Y. Chen, P. Li, Q. Liu and J. Wang, *Angewandte Chemie*, 2015, **127**, 14936-14940.
847 61. J. Li, S. Wang, J. Chang and L. Feng, *Advanced Powder Materials*, 2022, **1**, 100030.
848 62. C. Wang, H. Lu, Z. Mao, C. Yan, G. Shen and X. Wang, *Advanced Functional Materials*, 2020, **30**.
849 63. L. Meng, L. Li, J. Wang, S. Fu, Y. Zhang, J. Li, C. Xue, Y. Wei and G. Li, *Electrochimica Acta*,
850 2020, **350**, 136382.
851 64. Q. Li, W. Zhang, J. Shen, X. Zhang, Z. Liu and J. Liu, *Journal of Alloys and Compounds*, 2022,
852 **902**, 163670.
853 65. J. Cao, H. Li, R. Zhu, L. Ma, K. Zhou, Q. Wei and F. Luo, *Journal of Alloys and Compounds*, 2020,
854 **844**, 155382.
855 66. C. Chen, S. He, K. Dastafkan, Z. Zou, Q. Wang and C. Zhao, *Chinese Journal of Catalysis*, 2022,
856 **43**, 1267-1276.
857 67. K. Zhang, C. Liu, N. Graham, G. Zhang and W. Yu, *Nano Energy*, 2021, **87**.
858 68. Y. Qiu, X. Dai, Y. Wang, X. Ji, Z. Ma and S. Liu, *Journal of Colloid and Interface Science*, 2023,
859 **629**, 297-309.
860 69. C. Wang, X. Du and X. Zhang, *Journal of Alloys and Compounds*, 2022, **928**, 167094.
861 70. M. S. Amer, P. Arunachalam, A. M. Al-Mayouf, A. A. AlSaleh and Z. A. Almutairi, *Environmental*
862 *Research*, 2023, DOI: https://doi.org/10.1016/j.envres.2023.116818, 116818.
863 71. T. Wang, H. Wu, C. Feng, Y. Ding and H. Mei, *Electrochimica Acta*, 2021, **391**, 138931.
864 72. G. Liu, Z. Sun, D. Liu, Y. Li and W. Zhang, *Journal of Colloid and Interface Science*, 2023, **629**,
865 1012-1020.
866 73. Q. Xu, T. Yu, J. Chen, G. Qian, H. Song, L. Luo, Y. Chen, T. Liu, Y. Wang and S. Yin, *ACS Applied*
867 *Materials & Interfaces*, 2021, **13**, 16355-16363.
868 74. S. Gopi, A. Gopal Ramu, A. M. Al-Mohaimeed, D. Choi and K. Yun, *Materials Letters*, 2022, **308**,
869 131219.
870 75. J. Zhu, W. Lv, Y. Yang, L. Huang, W. Yu, X. Wang, Q. Han and X. Dong, *New Journal of Chemistry*,
871 2022, **46**, 10280-10288.
872 76. X. Xu, S. Ji, H. Wang, X. Wang, V. Linkov and R. Wang, *Journal of Colloid and Interface Science*,
873 2022, **615**, 163-172.
874 77. S. P. Selvam and S. Cho, *Advanced Sustainable Systems*, 2022, **6**, 2200038.
875 78. P. Balasubramanian, A. Jansirani, S.-B. He, H.-H. Deng, H.-P. Peng, X.-H. Xia and W. Chen,
876 *Journal of Power Sources*, 2021, **494**, 229757.
877 79. L. Lei, Z. Yin, D. Huang, Y. Chen, S. Chen, M. Cheng, L. Du and Q. Liang, *Journal of Colloid and*
878 *Interface Science*, 2022, **612**, 413-423.
879 80. G. Qian, J. Chen, L. Luo, H. Zhang, W. Chen, Z. Gao, S. Yin and P. Tsiakaras, *ACS Applied*
880 *Materials & Interfaces*, 2020, **12**, 38061-38069.

881   81.   X. Xu, X. Hou, P. Du, C. Zhang, S. Zhang, H. Wang, A. Toghan and M. Huang, *Nano Research*,
882   2022, **15**, 7124-7133.
883   82.   H. Xu, W.-D. Zhang, Y. Yao, J. Yang, J. Liu, Z.-G. Gu and X. Yan, *Journal of Colloid and Interface*
884   *Science*, 2023, **629**, 501-510.
885   83.   J. Jiang, H. Jiang, M. Chen, R. Ma, X. Wang, W. Wei and L. Ai, *Applied Surface Science*, 2022,
886   **600**, 154116.
887   84.   B. Kim, Y. Jung, B. J. Park, G. Das, H. H. Yoon and Y. S. Yoon, *International Journal of Hydrogen*
888   *Energy*, 2022, **47**, 5797-5806.
889   85.   P. Babar, A. Lokhande, V. Karade, B. Pawar, M. G. Gang, S. Pawar and J. H. Kim, *ACS Sustainable*
890   *Chemistry & Engineering*, 2019, **7**, 10035-10043.
891   86.   J. Tian, C. Cao, Y. He, M. I. Khan, X.-T. Wu and Q.-L. Zhu, *Green Energy & Environment*, 2022,
892   DOI: https://doi.org/10.1016/j.gee.2022.05.001.
893   87.   L. Chen, H. Wang, L. Tan, D. Qiao, X. Liu, Y. Wen, W. Hou and T. Zhan, *Journal of Colloid and*
894   *Interface Science*, 2022, **618**, 141-148.
895   88.   M. Yao, J. Ge, B. Sun, J. Hu, S. W. Koh, Y. Zhao, J. Fei, Z. Sun, W. Hong, Z. Chen, W. Hu and H.
896   Li, *Chemical Engineering Journal*, 2021, **414**, 128753.
897   89.   H. Sun, W. Zhang, J.-G. Li, Z. Li, X. Ao, K.-H. Xue, K. K. Ostrikov, J. Tang and C. Wang, *Applied*
898   *Catalysis B: Environmental*, 2021, **284**, 119740.
899   90.   C. Gao, G. Wei, C. Wang, X. Zhou, X. Zhao, Q. Zhao, S. Wang and F. Kong, *Journal of Alloys and*
900   *Compounds*, 2023, **959**, 170545.
901   91.   X. Wen, *International Journal of Hydrogen Energy*, 2020, **45**, 14660-14668.
902   92.   W. Liu, Z. Qin, X. Dai, S. Meng, X. Niu, W. Shi, F. Wu and X. Cao, *Energies*, 2023, **16**, 1092.
903   93.   K. Li and Y. Tong, *ChemCatChem*, 2022, **14**, e202201047.
904   94.   Y. Feng, X. Wang, J. Huang, P. Dong, J. Ji, J. Li, L. Cao, L. Feng, P. Jin and C. Wang, *Chemical*
905   *Engineering Journal*, 2020, **390**, 124525.
906   95.   J. Zhao, Y. Zhang, H. Guo, J. Ren, H. Zhang, Y. Wu and R. Song, *Chemical Engineering Journal*,
907   2022, **433**, 134497.
908   96.   Q. Li, Q. Chen, S. Lei, M. Zhai, G. Lv, M. Cheng, L. Xu, H. Xu, Y. Deng and J. Bao, *Journal of*
909   *Colloid and Interface Science*, 2023, **631**, 56-65.
910   97.   X. F. Lu, S. L. Zhang, W. L. Sim, S. Gao and X. W. Lou, *Angewandte Chemie International Edition*,
911   2021, **60**, 22885-22891.
912   98.   H. Wang, X. Jiao, W. Zeng, Y. Zhang and Y. Jiao, *International Journal of Hydrogen Energy*, 2021,
913   **46**, 37792-37801.
914   99.   S. Wei, X. Wang, J. Wang, X. Sun, L. Cui, W. Yang, Y. Zheng and J. Liu, *Electrochimica Acta*, 2017,
915   **246**, 776-782.
916   100.   Z. Jiang, L. Zheng, M. Liu, H. Xu, S. Chen, F. Xiong, Y. Liao, Y. Liao, Y. Qing and Y. Wu, *Applied*
917   *Surface Science*, 2023, **638**, 158058.
918   101.   W. Liu, L. Dai, Y. Hu, K. Jiang, Q. Li, Y. Deng, J. Yuan, J. Bao and Y. Lei, *Inorganic Chemistry*
919   *Frontiers*, 2021, **8**, 4528-4535.
920   102.   W. Zhu, Z. Yue, W. Zhang, N. Hu, Z. Luo, M. Ren, Z. Xu, Z. Wei, Y. Suo and J. Wang, *Journal of*
921   *Materials Chemistry A*, 2018, **6**, 4346-4353.
922   103.   M. Liu, Y. Jiao, S. Zhan and H. Wang, *Catalysis Today*, 2020, **355**, 596-601.
923   104.   W. Song, M. Xu, X. Teng, Y. Niu, S. Gong, X. Liu, X. He and Z. Chen, *Nanoscale*, 2021, **13**, 1680-
924   1688.
925   105.   S. A. Patil, H. T. Bui, S. Hussain, I. Rabani, Y. Seo, J. Jung, N. K. Shrestha, H. Kim and H. Im,
926   *Dalton Transactions*, 2021, **50**, 12723-12729.
927   106.   H. Xu, K. Ye, K. Zhu, Y. Gao, J. Yin, J. Yan, G. Wang and D. Cao, *Inorganic Chemistry Frontiers*,
928   2021, **8**, 2788-2797.
929   107.   H. Xu, K. Ye, J. Yin, K. Zhu, J. Yan, G. Wang and D. Cao, *Journal of Power Sources*, 2021, **491**,
930   229592.
931   108.   F. Wang, K. Zhang, Q. Zha and Y. Ni, *Journal of Alloys and Compounds*, 2022, **899**, 163346.

49

932 109. Y. Jiang, S. Gao, G. Xu and X. Song, *Journal of Materials Chemistry A*, 2021, **9**, 5664-5674.
933 110. H. Zhang, Y. Qiu, S. Zhang, Q. Liu, J. Luo and X. Liu, *Ionics*, 2022, **28**, 3927-3934.
934 111. D. Li, W. Wan, Z. Wang, H. Wu, S. Wu, T. Jiang, G. Cai, C. Jiang and F. Ren, *Advanced Energy*
935   *Materials*, 2022, **12**, 2201913.
936 112. H. Xu, Y. Liao, Z. Gao, Y. Qing, Y. Wu and L. Xia, *Journal of Materials Chemistry A*, 2021, **9**,
937   3418-3426.
938 113. M. Maleki, G. Barati Darband, A. Sabour Rouhaghdam, R. Andaveh and Z. Mohammad Kazemi,
939   *Chemical Communications*, 2022, **58**, 3545-3548.
940 114. Z. Zhao, L. Yang, Z. Wang, L. Wang, G. Guo, J. Chen, Y. Li, C. Wang, J. Zhao and Z. Cai, *Journal*
941   *of The Electrochemical Society*, 2020, **167**, 126514.
942 115. X. Zhuo, W. Jiang, G. Qian, J. Chen, T. Yu, L. Luo, L. Lu, Y. Chen and S. Yin, *ACS Applied*
943   *Materials & Interfaces*, 2021, **13**, 35709-35718.
944 116. V. Maheskumar, K. Saravanakumar, Y. Yea, Y. Yoon and C. M. Park, *International Journal of*
945   *Hydrogen Energy*, 2023, **48**, 5080-5094.
946 117. S. Ligani Fereja, P. Li, Z. Zhang, J. Guo, Z. Fang, Z. Li, S. He and W. Chen, *Chemical Engineering*
947   *Journal*, 2022, **432**, 134274.
948 118. R. Wang, J. Cao, R. Zhang, Z. Sun, F. Wang and H. Wu, *International Journal of Hydrogen Energy*,
949   2022, **47**, 29593-29603.
950 119. N. Chen, X. Du and X. Zhang, *Renewable Energy*, 2022, **193**, 715-724.
951 120. Z. Jiang, L. Zheng, C. Sheng, H. Xu, S. Chen, Y. Liao, Y. Qing and Y. Wu, *Journal of Colloid and*
952   *Interface Science*, 2022, **626**, 848-857.
953 121. Z. Wang, P. Guo, M. Liu, C. Guo, H. Liu, S. Wei, J. Zhang and X. Lu, *ACS Applied Energy*
954   *Materials*, 2019, **2**, 3363-3372.
955 122. Y. Zhang, Y. Qiu, Y. Wang, B. Li, Y. Zhang, Z. Ma and S. Liu, *ACS Applied Materials & Interfaces*,
956   2021, **13**, 3937-3948.
957 123. H. Yu, S. Zhu, Y. Hao, Y.-M. Chang, L. Li, J. Ma, H.-Y. Chen, M. Shao and S. Peng, *Advanced*
958   *Functional Materials*, 2023, **33**, 2212811.
959 124. Q. Wen, K. Yang, D. Huang, G. Cheng, X. Ai, Y. Liu, J. Fang, H. Li, L. Yu and T. Zhai, *Advanced*
960   *Energy Materials*, 2021, **11**, 2102353.
961 125. Y. Ren, C. Wang, W. Duan, L. Zhou, X. Pang, D. Wang, Y. Zhen, C. Yang and Z. Gao, *Journal of*
962   *Colloid and Interface Science*, 2022, **628**, 446-455.
963 126. C. Gu, G. Zhou, J. Yang, H. Pang, M. Zhang, Q. Zhao, X. Gu, S. Tian, J. Zhang, L. Xu and Y. Tang,
964   *Chemical Engineering Journal*, 2022, **443**, 136321.
965 127. V. T. Veettil, A. U. Vijayakumar, A. Ashdot and D. Zitoun, *ACS Applied Energy Materials*, 2022, **5**,
966   1397-1402.
967 128. Z. Zhao, J. Zhao, H. Wang, X. Li, L. Yang, Z. Zhao, X. Liu, Y. Liu, P. Liu and Z. Cai, *International*
968   *Journal of Hydrogen Energy*, 2020, **45**, 14199-14207.
969 129. D. Liu, T. Liu, L. Zhang, F. Qu, G. Du, A. M. Asiri and X. Sun, *Journal of Materials Chemistry A*,
970   2017, **5**, 3208-3213.
971 130. R. Tong, M. Xu, H. Huang, J. Wu, Y. Xiong, M. Shao, Y. Zhao, S. Wang and H. Pan, *International*
972   *Journal of Hydrogen Energy*, 2022, **47**, 11447-11455.
973 131. L. Sha, J. Yin, K. Ye, G. Wang, K. Zhu, K. Cheng, J. Yan, G. Wang and D. Cao, *Journal of Materials*
974   *Chemistry A*, 2019, **7**, 9078-9085.
975 132. H. Xu, K. Ye, K. Zhu, Y. Gao, J. Yin, J. Yan, G. Wang and D. Cao, *ACS Sustainable Chemistry &*
976   *Engineering*, 2020, **8**, 16037-16045.
977 133. T. I. Singh, G. Rajeshkhanna, S. B. Singh, T. Kshetri, N. H. Kim and J. H. Lee, *ChemSusChem*,
978   2019, **12**, 4810-4823.
979 134. N. Sinha and P. Roy, *Inorganic Chemistry*, 2023, **62**, 3349-3357.
980 135. L. Yang and L. Zhang, *Journal of Colloid and Interface Science*, 2022, **607**, 546-555.
981 136. J. Cao, Z. Jiao, R. Zhu, H. Long, Y. Zheng, J. Pan, J. Wang, F. Luo, C. Li and Q. Wei, *Journal of*
982   *Alloys and Compounds*, 2022, **914**, 165362.

983 137. R.-Q. Li, Q. Liu, Y. Zhou, M. Lu, J. Hou, K. Qu, Y. Zhu and O. Fontaine, *Journal of Materials*
984 *Chemistry A*, 2021, **9**, 4159-4166.
985 138. Y. Liu, D. Zheng, Y. Zhao, P. Shen, Y. Du, W. Xiao, Y. Du, Y. Fu, Z. Wu and L. Wang, *International*
986 *Journal of Hydrogen Energy*, 2022, **47**, 25081-25089.
987 139. H. Jiang, M. Sun, S. Wu, B. Huang, C. S. Lee and W. Zhang, *Advanced Functional Materials*, 2021,
988 DOI: 10.1002/adfm.202104951.
989 140. F. Wang, D. Zhao, L. Zhang, L. Fan, X. Zhang and S. Hu, *Nanomaterials*, 2019, **9**, 1583.
990 141. M. Zabihinezhad, T. Shahrabi, C. Zheng, T. Shao, G. Barati Darband and J. Li, *Journal of*
991 *Electroanalytical Chemistry*, 2023, **942**, 117528.
992 142. Y. Tong, L. Chen, P. J. Dyson and Z. Fei, *Journal of Materials Science*, 2021, **56**, 17709-17720.
993 143. X. Lan, G. Li, R. Jin, X. Li and J. Zheng, *Chemical Engineering Journal*, 2022, **450**, 138225.
994 144. J. Xiao, R. Tan, Y. Guo, P. Zhao and X. Luo, *International Journal of Hydrogen Energy*, 2022, **47**,
995 28730-28739.
996 145. J. Zheng, K. Wu, C. Lyu, X. Pan, X. Zhang, Y. Zhu, A. Wang, W.-M. Lau and N. Wang, *Applied*
997 *Surface Science*, 2020, **506**, 144977.
998 146. Y. Zhou, B. Chu, Z. Sun, L. Dong, F. Wang, B. Li, M. Fan and Z. Chen, *Applied Catalysis B:*
999 *Environmental*, 2023, **323**, 122168.
1000 147. L. Meng, L. Zhang, S. Liu, F. Wang and H. Wu, *International Journal of Hydrogen Energy*, 2023,
1001 DOI: https://doi.org/10.1016/j.ijhydene.2023.05.143.
1002 148. B. Chen, M. Humayun, Y. Li, H. Zhang, H. Sun, Y. Wu and C. Wang, *ACS Sustainable Chemistry*
1003 *& Engineering*, 2021, **9**, 14180-14192.
1004 149. J. Liu, Y. Wang, Y. Liao, C. Wu, Y. Yan, H. Xie and Y. Chen, *ACS Applied Materials & Interfaces*,
1005 2021, **13**, 26948-26959.
1006 150. P. Yi, Y. Song, C. Li, R. Liu and J. Sun, *Applied Surface Science*, 2023, **619**, 156789.
1007 151. T. Wang, L. Miao, S. Zheng, H. Qin, X. Cao, L. Yang and L. Jiao, *ACS Catalysis*, 2023, **13**, 4091-
1008 4100.
1009 152. B. Lu, D. Wang, C. Zhao, K. Zhu, J. Yan, G. Wang, D. Cao and K. Ye, *Materials Chemistry*
1010 *Frontiers*, 2022, **6**, 1681-1689.
1011 153. L. Jiang, Y. Pan, J. Zhang, X. Chen, X. Ye, Z. Li, C. Li and Q. Sun, *Journal of Colloid and Interface*
1012 *Science*, 2022, **622**, 192-201.
1013 154. T. Wang, H. Wu, C. Feng, L. Zhang and J. Zhang, *Journal of Materials Chemistry A*, 2020, **8**,
1014 18106-18116.
1015 155. R. Wang, T. Wnag, C. Feng, H. Wu, Y. Ding and H. Me, *International Journal of Hydrogen Energy*,
1016 2021, **46**, 38247-38257.
1017 156. D. Khalafallah, A. A. Farghaly, C. Ouyang, W. Huang and Z. Hong, *Journal of Power Sources*,
1018 2023, **558**, 232563.
1019 157. H. Wang, H. Zou, Y. Liu, Z. Liu, W. Sun, K. A. Lin, T. Li and S. Luo, *Scientific Reports*, 2021, **11**,
1020 21414.
1021 158. C. Chen, L. Jin, L. Hu, T. Zhang, J. He, P. Gu, Q. Xu and J. Lu, *Journal of Colloid and Interface*
1022 *Science*, 2022, **628**, 1008-1018.
1023 159. Y. Wang, C. Wang, H. Shang, M. Yuan, Z. Wu, J. Li and Y. Du, *Journal of Colloid and Interface*
1024 *Science*, 2022, **605**, 779-789.
1025 160. Z. Liu, S. Xue, S. Zhou, J. Li, K. Qu and W. Cai, *Journal of Catalysis*, 2022, **405**, 606-613.
1026 161. L. Zhang, Y. Wang, J. Cao, R. Zhang, F. Wang and H. Wu, *International Journal of Hydrogen*
1027 *Energy*, 2022, **47**, 34715-34726.
1028 162. N. T. Nguyen, T. T. N. Tran, T.-K. Truong, J. Yu, T. N.-M. Le, T. B. Phan, T. L. H. Doan, L. H. T.
1029 Nguyen, T. D. Luong, T.-H. Nguyen and N. Q. Tran, *Inorganic Chemistry*, 2023, **62**, 10298-10306.
1030 163. K. Wu, H. Li, C. Lyu, J. Cheng, Y. Yang, X. Zhu, W.-M. Lau and J. Zheng, *Journal of Alloys and*
1031 *Compounds*, 2023, **945**, 169290.
1032 164. X. Du, Y. Ding and X. Zhang, *Green Energy & Environment*, 2023, **8**, 798-811.
1033 165. C. Zhang, X. Du and X. Zhang, *International Journal of Hydrogen Energy*, 2022, **47**, 10825-10836.

1034   166.   Y. Xu, T. Ren, K. Ren, S. Yu, M. Liu, Z. Wang, X. Li, L. Wang and H. Wang, *Chemical Engineering*
1035   *Journal*, 2021, **408**.
1036   167.   H. Liu, D. Wen and B. Zhu, *Journal of Electroanalytical Chemistry*, 2023, **928**, 117082.
1037   168.   K. Xiong, L. Yu, Y. Xiang, H. Zhang, J. Chen and Y. Gao, *Journal of Alloys and Compounds*, 2022,
1038   **912**, 165234.
1039   169.   A. Nadeema, V. Kashyap, R. Gururaj and S. Kurungot, *ACS Applied Materials & Interfaces*, 2019,
1040   **11**, 25917-25927.

1041